Supplemental Material for

Investigating the global and regional response of drought to idealized deforestation using multiple global climate models

Yan Li[1], Bo Huang[2], Chunping Tan[3], Xia Zhang[2], Francesco Cherubini[2], and Henning W. Rust[1]

[1] Institute of Meteorology, Freie Universität Berlin, 12165, Berlin, Germany

[2] Department of Energy and Process Engineering, Norwegian University of Science and Technology, 7491, Trondheim, Norway

[3] Institute for Disaster Management and Reconstruction, Sichuan University, 610200 Chengdu, China

Corresponding author: Bo Huang, bo.huang@ntnu.no

Supplementary Text 1

BCC-CSM2-MR

The land model employed in BCC-CSM2-MR is the Beijing Climate Center Atmosphere and Vegetation Interaction Model (BCC_AVIM) (Li et al. 2019). BCC_AVIM is a comprehensive land surface model seamlessly integrated into BCC-CSM-CSM to simulate a range of land surface biogeophysical and plant ecophysiological processes (Wu et al. 2019; Wu et al. 2013). This model facilitates the dynamic exchange of energy, water, and carbon between the land surface and the atmosphere. Within BCC_AVIM, the terrestrial carbon cycle operates through a series of biochemical and physiological processes, particularly focusing on photosynthetic assimilation and vegetation respiration. Notably, BCC_AVIM incorporates a dynamic scheme for determining leaf unfolding, growth, and withering dates. This scheme aligns with the budget of photosynthetically assimilated carbon, resembling a phenology scheme. The model thus captures the intricate dynamics of vegetation development and carbon cycling within the land-atmosphere interface.

CMCC-ESM2

The CMCC-ESM2 was developed and executed by the Fondazione Centro Euro-Mediterraneo sui Cambiamenti Climatici, based in Lecce, Italy (CMCC), at native nominal resolutions of 100 km for all components (Lovato et al. 2022). The terrestrial biogeochemical processes in CMCC-ESM2 are represented by the Community Land Model version 4.5 (CLM4.5) in its biogeochemical (BGC) configuration including key processes concerning global carbon and nitrogen cycles (Koven et al. 2013; Oleson et al. 2013). Photosynthesis descriptions vary among plant types, with C3 plants modeled (Farquhar et al. 1980) and C4 plants (Collatz et al. 1992). These methods differ in leaf-level parameterization of carboxylation and limiting factors. The resulting photosynthate is allocated into various vegetation carbon pools, and the transfer of carbon into litter-soil pools follows a dynamic cascade (Parton et al. 1988). Decomposition rates, including CO2 release, are influenced by the vegetation spatial distribution, which is represented by 15 plant functional types (PFTs). The phenology, or seasonal growth and litterfall, responds prognostically to environmental factors such as soil and air temperature, soil moisture, and day length. Additionally, CLM4.5-BGC incorporates a fire module that characterizes different fire components, including non-peat fires, agricultural fires, deforestation fires in tropical closed forests, and peat fires. Burned area estimation considers climate conditions, vegetation characteristics, and human activities.

Compared to the previous CMCC-ESM2 version (SILVA), which relied on VEGAS parameterizations,

CLM4.5-BGC offers enhancements such as an increased number of carbon pools in vegetation representation, extended decomposition cascades, and heightened vegetation heterogeneity with 15 PFTs instead of 4. Notably, CMCC-ESM2 includes a prognostic representation of the nitrogen cycle, considering inputs from atmospheric deposition and biological nitrogen fixation. Nitrogen storage and allocation within vegetation follow established carbon to nitrogen ratios, while losses occur through processes such as nitrification, denitrification, leaching, and fire. Nitrogen availability also affects decomposition rates, illustrating the interconnectedness of carbon and nitrogen cycles within terrestrial ecosystems.

CNRM-ESM2-1

CNRM-ESM2-1, the second-generation Earth System model for CMIP6 developed by CNRM-CERFACS, features a comprehensive set of components to simulate various Earth system processes (Séférian et al. 2019). The atmospheric core is represented by ARPEGE-Climat_v6.3 (Roehrig et al. 2020), coupled with the NEMOv3.6 ocean model that includes the GELATOv6.0 sea-ice model and the PISCES-v2-gas ocean biogeochemistry model (Berthet et al. 2019). The land surface is characterized by the ISBA-CTRIP land surface model (Decharme et al. 2019; Delire et al. 2020), and surface state variables and fluxes are simulated by the SURFEX modeling platform version 8.0, operating on the same grid and time-step as the atmospheric model. SURFEXv8.0 encompasses submodules for modeling interactions between the atmosphere, ocean, lakes, and land surface.

Over the land surface, ISBA-CTRIP solves energy, carbon, and water budgets, explicitly considering the one-dimensional Fourier and Darcy laws throughout the soil. A 12-layer snow model accounts for separate water and energy budgets in the soil and snowpack. The land model includes a dynamic river flooding scheme, incorporating interactions between floodplains, soil, and the atmosphere. It also features a two-dimensional diffusive groundwater scheme to represent unconfined aquifers and upward capillarity fluxes into the superficial soil (Decharme et al. 2019). To simulate the land carbon cycle and vegetation-climate interactions, ISBA-CTRIP includes modules for plant physiology, carbon allocation and turnover, and carbon cycling through litter and soil. It incorporates a module for wildfires, land use and land cover changes, and carbon leaching through the soil with transport of dissolved organic carbon to the ocean. Leaf photosynthesis is represented by the semi-empirical model (Goudriaan et al. 1985), and canopy-level assimilation is calculated using a 10-layer radiative transfer scheme. Vegetation in ISBA is represented by four carbon pools for grasses and crops and two additional pools for trees. Sixteen vegetation types are distinguished, including tree and shrub types, grass types, crop types, as

well as desert, rocks, and permanent snow. Nitrogen cycling within vegetation is absent, but an implicit nitrogen limitation scheme, reducing specific leaf area with increasing CO2 concentration, is implemented based on the meta-analysis of Yin (2002). Additionally, an ad-hoc representation of photosynthesis down-regulation is included. The litter and soil organic matter module is based on the soil carbon component of the CENTURY model (Parton et al. 1988), defining four litter and three soil carbon pools based on their location and potential decomposition rates. Decomposition releases CO2 as heterotrophic respiration, and dissolved organic carbon resulting from this process is transported by rivers to the ocean (Delire et al. 2020).

CanESM5

CanESM5, an evolution from its predecessor CanESM2, has undergone significant improvements in various components, particularly in the ocean, sea-ice, marine ecosystems, and the coupler (Swart et al. 2019). Notable changes relative to CanESM2 include the introduction of entirely new models for the ocean, sea-ice, marine ecosystems, and a new coupler. Despite these advancements, the resolution of CanESM5 (T63 or approximately 2.8° in the atmosphere and ~1° in the ocean) remains similar to CanESM2. Various improvements have been implemented in the atmospheric component of CanESM5, encompassing changes to aerosol, clouds, radiation, land surface, and lake processes. CanESM5 now employs 49 atmospheric levels compared to the 35 levels in CanESM2, with the additional 14 levels primarily concentrated in the upper troposphere and stratosphere.

The land surface in CanESM5 is modeled using the Canadian Land Surface Scheme (CLASS) and the Canadian Terrestrial Ecosystem Model (CTEM), forming the land component of CanESM5. CLASS and CTEM jointly simulate physical and biogeochemical land surface processes, calculating fluxes of energy, water, CO2, and wetland CH4 emissions at the land-atmosphere boundary. Over land, three permeable soil layers with default thicknesses of 0.1, 0.25, and 3.75 meters are employed, with prognostically calculated liquid and frozen soil moistures and temperatures. The depth to bedrock is specified based on a global dataset, adjusting thicknesses of permeable soil layers where soil depth is less than 4.1 meters. Snow in CLASS is represented by one layer with prognostically modeled snow water equivalent and temperature. The introduction of dynamic wetlands and associated methane emissions is a new biogeochemical process introduced since CanESM2. CTEM simulates photosynthesis, prognostically calculating carbon amounts in three live (leaves, stem, and root) and two dead (litter and soil) carbon pools. The nitrogen cycle over land is not represented, but a parameterization of photosynthesis down-regulation with increasing CO2 concentration is included.

EC-Earth-veg

EC-Earth-Veg v3.3.1.1 (Döscher et al. 2022; Wyser et al. 2020a; Wyser et al. 2020b) is a subconfiguration of the Consortium Earth-system model EC-Earth (Hazeleger et al. 2012), integrating the atmospheric model IFS cycle 36r4 with the Land-Surface model HTESSEL (Boussetta et al. 2013), the ocean model NEMO3.6 (Vancoppenolle et al. 2009) including the sea-ice model LIM3, and the dynamic global vegetation and biogeochemistry model LPJ-GUESSv4.0 (Lindeskog et al. 2013; Olin et al. 2015; Smith et al. 2014). The coupling between these components is facilitated by the OASIS3-MCT coupling library (Craig et al. 2017), with a standard resolution applied.

In this configuration, HTESSEL and LPJ-GUESS act as a combined land-surface scheme, with LPJ-GUESS simulating vegetation dynamics, management, land use, terrestrial carbon and nitrogen cycles, and incorporating six stand-types (Natural, Pasture, Urban, Crop, Irrigated Crop, and Peatland). LPJ-GUESS features competition among plant functional types (PFTs) within each stand-type, with tree establishment disabled on deforested areas, leaving only herbaceous PFTs in competition. The model represents global carbon and nitrogen cycles within vegetation, litter, and soil organic matter pools, influencing soil biogeochemistry, CO2 fluxes, and nitrogen trace gas emissions. Water cycling in LPJ-GUESS is decoupled from the rest of EC-Earth due to differing evaporation and hydrology schemes compared to HTESSEL. While HTESSEL updates a single soil water pool per gridcell based on aggregated water fluxes, LPJ-GUESS calculates evapotranspiration independently in each patch and stand within every gridcell, reflecting sub-grid scale heterogeneity of hydrological cycling and ecosystem functioning. Deforestation is implemented annually, converting primary forest to secondary forest where tree establishment is disabled. LPJ-GUESS evaluates vegetation removal within deforested areas, leaving a portion of leaves, wood, and roots on site transferred into the litter.

GISS-E2-1-G

The GISS-E2-1-G, developed by NASA's Goddard Institute for Space Studies, is an earth system model encompassing various land surface processes (Kelley et al. 2020). These processes include infiltration, soil water flow, evaporation from bare soil, transpiration, evaporation from intercepted precipitation and dew, and throughfall. The model effectively manages both surface and underground runoff. Additionally, it incorporates subgrid scale distribution of precipitation and surface runoff. Key features of the model include the consideration of frozen soil layers and snow cover on the canopy and soil. Operating on a one-dimensional framework for each grid box, the model divides the surface and

underlying ground into bare and vegetated regions, which are conceptualized as interspersed. The vegetative canopy is represented as a single layer with specific heat capacity, while the soil under both bare and vegetated regions is structured into six layers. Evaporative and heat fluxes between the land surface and an atmospheric reference layer are calculated within the model (Rosenzweig and Abramopoulos 1997). Moreover, canopy stomatal conductance and photosynthesis are updated using a physiology-based model, enabling a comprehensive understanding of vegetation dynamics and their interaction with the environment (Friend and Kiang 2005).

IPSL-CM6A-LR

IPSL-CM6A-LR, developed by the Institut Pierre-Simon Laplace Climate Modelling Centre (IPSL CMC) for the CMIP6 exercise, is comprised of three main components: the LMDZ atmospheric model version 6A-LR, the NEMO oceanic model version 3.6, and the ORCHIDEE land surface model version 2.0 (Boucher et al. 2020).

In terms of vegetation representation, IPSL-CM6A-LR incorporates 15 Plant Functional Types (PFTs), including 8 for trees, 4 for grasses, 2 for crops, and 1 for bare soil. In the CMIP6 configuration, vegetation distribution within each grid cell is prescribed by land cover maps, and only net land-use changes are considered. For soil water dynamics, three independent soil water columns are computed per grid cell, grouping together PFTs with similar properties: one for bare soil, one for trees, and another for short-vegetation types. Vertical water fluxes, accounting for hydraulic conductivity and diffusivity, are calculated using an 11-layer soil hydrology scheme down to 2 meters, with a free drainage condition at the bottom of the soil column (de Rosnay et al. 2002). In contrast to the water budget, IPSL-CM6A-LR solves a single energy budget per grid cell, resulting in a single computed surface temperature without distinguishing temperatures for different PFTs within a grid cell. Albedo values for soil, snow, and vegetation for various PFTs are determined through an optimization procedure using remote sensing albedo data from the MODIS sensor. Biomass modeling in IPSL-CM6A-LR focuses solely on carbon, excluding considerations for nitrogen and other nutrient-related limitations. The assimilation of carbon through photosynthesis and its flow within the plant-soil continuum are governed by equations outlined in Krinner et al. (2005). Living biomass is represented by six main pools, including leaf, fine roots, sapwood, heartwood above and below ground. Soil carbon biomass follows the CENTURY model (Parton et al. 1988), incorporating three pools with different decomposition times (active, slow, and passive pools). The model does not account for carbon removal due to fire activity.

MIROC-ES2L

The MIROC-ES2L model builds upon the global climate model MIROC5.2 (Tatebe et al. 2018), which integrates various components, including an atmospheric general circulation model (CCSR-NIES AGCM, Tatebe et al. 2019) with an on-line aerosol component (SPRINTARS, Takemura et al. 2000), an ocean GCM with a sea-ice component (COCO, Hasumi, 2006), and a land physical surface model (MATSIRO, Takata et al. 2003). Additionally, it incorporates the VISIT land biogeochemical component and OECO2 ocean biogeochemical component (Ito and Inatomi 2012).

Within MIROC-ES2L, two land components, MATSIRO and VISIT, are coupled via soil water content, runoff, and leaf area index (Arora et al. 2020; Hajima et al. 2020). The model captures the terrestrial carbon cycle, including vegetation (leaf, stem, and root), litter (leaf, stem, and root), and humus (active, intermediate, and passive) pools, with biome distribution fixed based on MODIS vegetation cover categories. Detailed information on carbon cycle processes can be found in Ito and Oikawa (2002). Moreover, MIROC-ES2L simulates the nitrogen cycle, considering pools of vegetation (canopy and structural), organic soil (litter, humus, and microbe), and inorganic nitrogen (ammonium and nitrate). Photosynthetic capacity in the model is regulated by leaf nitrogen concentration (Arora et al. 2020; Hajima et al. 2020). Land-use change (LUC) impacts are modeled in MIROC-ES2L, assuming two types of impacts on biogeochemistry. Firstly, even with fixed areal fractions, such as during spin-up runs under 1850 conditions, processes like crop harvesting, nitrogen fixation by N-fixing crops, and organic matter decay in product pools occur. Secondly, when the areal fraction changes within a year, carbon and nitrogen from harvested biomass are translocated between product pools. For instance, when cropland is abandoned and reclassified as secondary forest, the mean mass density of secondary forest initially dilutes due to increased less-vegetated area, followed by regrowth towards a new stabilization state (Hajima et al. 2020).

UKESM1-0-LL

UKESM1-0-LL, the low-resolution variant of the UK Earth System Model, comprises several components (Sellar et al. 2019). The atmospheric core is formed by the Met Office Unified Model at vn11.2, coupled with the NEMO ocean model (vn3.6) incorporating the MEDUSA ocean biogeochemistry model version 2.0 (Yool et al. 2013). The land surface is represented by version 5.0 of the JULES land surface model (Clark et al. 2011).

JULES includes nine natural Plant Functional Types (PFTs), encompassing three broadleaf trees, two needleleaf trees, two shrubs, and two grasses (Harper et al. 2016), along with four additional PFTs

dedicated to agriculture (C3 and C4 crop and pasture, Burton et al. 2019). Natural and agricultural PFTs are segregated within the grid box, with the dynamic vegetation model, TRIFFID, enabling competition among PFTs within each unit based on evolving climate conditions. However, there is no competition between natural and agricultural PFTs, preventing natural vegetation from repopulating agricultural regions.

The soil carbon component of JULES is based on the RothC four-pool soil Carbon model (Coleman et al. 1997), comprising Decomposable Plant Material, Resistant Plant Material, Biomass, and Humus pools, each with distinct decay rates. Plant litter contributes to the Decomposable Plant Material and Resistant Plant Material pools, with carbon transferring to Biomass and Humus pools for continued decay, releasing CO2. Version 5.0 of JULES incorporates nitrogen limitation of carbon uptake by plants, featuring four organic soil nitrogen pools mirroring the soil carbon pools, and an inorganic soil nitrogen pool. Nitrogen demand by plants is calculated from the C:N ratio and Net Primary Productivity (NPP), with the inorganic nitrogen pool replenished by biogenic nitrogen fixation and atmospheric nitrogen deposition. Crop PFTs are assumed to be perfectly fertilized, with their N demand met and NPP not downregulated, constituting an implicit nitrogen fertilization flux. A portion of crop litter is intercepted, representing a harvest flux. Pasture PFTs are unfertilized and not subject to removal by harvest or grazing. In CO2 concentration-driven mode, the CO2 flux from wood product pool decay, harvest flux, and unassimilated NPP carbon are diagnostic-only. In CO2 emissions-driven configuration, they contribute to a CO2 flux directly added to the atmospheric CO2 store.

Table S1. Variables used in the calculation of SPEI.

Variable abbreviation	Variable full name	Units in LUMIP	units in calculation of SPEI
pr	Precipitation	$kg\ m^{-2}\ s^{-1}$	mm
tasmax	Daily maximum near-surface air temperature	K	℃
taxmin	Daily minimum near-surface air temperature	K	℃
uas	Eastward near-surface wind	$m\ s^{-1}$	$m\ s^{-1}$
vas	Northward near-surface wind	$m\ s^{-1}$	$m\ s^{-1}$
lat	Latitude	degrees north	degrees north
ps	Surface air pressure	Pa	kPa
clt	Total cloud cover percentage	%	%

Table S2. Introduction of the participating models

Model Name	Spatial resolution	Dynamic vegetation module	Note	Simulation DOI	Nation
BCC-CSM2-MR	1.125°x1.1°	no	ΔtreeFrac = 1900-1850 piControl year 2289	https://doi.org/10.22033/ESGF/CMIP6.1730	China
CMCC-ESM2	0.94°x1.25°	no	piControl year 1850	https://doi.org/10.22033/ESGF/CMIP6.13166	Italy
CNRM-ESM2-1	1.4°x1.4°	no	cSoil = slow + medium + fast Separate file for ΔtreeFrac piControl year 1850	https://doi.org/10.22033/ESGF/CMIP6.1393	France
CanESM5	2.8°x 2.8°	no	piControl year 5700	http://doi.org/10.22033/ESGF/CMIP6.1313	Canada
EC-Earth3-veg	0.7°x0.7°	both	Annual maximum of ΔtreeFrac; separate file for deforestation mask; cSoil = slow + medium + fast piControl year 1930	http://doi.org/10.22033/ESGF/CMIP6.692	Europe
GISS-E2-1-G	2.5°x2.5°	no	piControl year 1850	http://doi.org/10.22033/ESGF/CMIP6.7040	USA
IPSL-CM6A-LR	1.27°x2.5°	no	Deforested grid cells are selected on a area (of forest) basis, not on a fraction (of forest) basis piControl years 1870, 1910, 1950	http://doi.org/10.22033/ESGF/CMIP6.1528	France
MIROC-ES2L	2.8°x2.8°	no	No prescribing of land cover types possible (forest regrowth); separate file for deforestation mask; piControl year 1850	http://doi.org/10.22033/ESGF/CMIP6.922	Japan
UKESM1-0-LL	1.25°x1.87°	both	ΔtreeFrac = 1900-1850 piControl year 1960	http://doi.org/10.22033/ESGF/CMIP6.1564	United Kingdom

Table S3. Mean and Standard deviation (SD) of global and regional changes (*deforest-global* minus *piControl*) in forest fraction (unit: %), precipitation (unit: mm yr^{-1}), and temperature (unit: °C) for the later 30 years, based on nine LUMIP models (BCC-CSM2-MR, CMCC-ESM2, CNRM-ESM2-1, CanESM5, EC-Earth3-Veg, GISS-E2-1-G, IPSL-CM6A-LR, MIROC-ES2L, and UKESM1-0-LL), and multi-model ensemble mean (MME) results.

		Forest Fraction (%)		Precipitation (mm yr^{-1})		Temperature (°C)	
		Mean	SD	Mean	SD	Mean	SD
BCC-CSM2-MR	Global			-1.5	8.67	-0.35	0.23
	Tropical			18.75	56.31	0.07	0.22
	Dry			3.33	21.52	-0.19	0.27
	Temperate			-3.86	34.24	-0.17	0.21
	Continental			-4.37	19.58	-0.37	0.81
	Polar			-7.75	7.7	-0.59	0.48
CMCC-ESM2	Global	-12.41	0	-4.06	18.37	-0.51	0.38
	Tropical	-34.69	0	5.2	119.35	0.03	0.46
	Dry	-0.12	0	3.81	28.43	-0.4	0.42
	Temperate	-13.44	0	0.44	32.2	-0.37	0.24
	Continental	-16.03	0	-16.02	18.97	-1.3	0.73
	Polar	-0.23	0	-4.73	9.79	-0.3	0.45
CNRM-ESM2-1	Global	-7.18	0	-0.71	8.4	-0.49	0.26
	Tropical	-17.74	0	-34.79	57.91	-0.18	0.27
	Dry	-0.37	0	8.69	21.95	-0.37	0.22
	Temperate	-13.67	0	-2.21	36.06	-0.45	0.19
	Continental	-15.62	0	17.9	12.3	-1.05	0.63
	Polar	-0.06	0	-4.64	8.35	-0.33	0.53
CanESM5	Global	-10.59	0	-20.41	12.01	-0.86	0.24
	Tropical	-25.82	0	-42.49	73.68	-0.05	0.31
	Dry	-1.25	0	-7.57	23	-0.47	0.21
	Temperate	-17.463	0	-28.9	28.96	-0.51	0.19
	Continental	-23.52	0	-25.45	16.54	-1.98	0.58
	Polar	-0.35	0	-13.75	5.21	-0.72	0.39
EC-Earth3-Veg	Global	-8.73	0.21	-2.79	10.36	-0.4	0.31
	Tropical	-32.03	0.65	-5.72	48.57	-0.19	0.22
	Dry	-2	0.56	0.45	24.86	-0.31	0.24
	Temperate	-19.27	0.5	4.47	30.7	-0.46	0.31
	Continental	-11.01	0.34	-10.78	15.31	-0.97	0.63
	Polar	-0.02	0	-0.62	9.26	-0.16	0.53
GISS-E2-1-G	Global			-22.42	6.68	-0.73	0.3
	Tropical			-81.38	68.29	-0.37	0.46
	Dry			-10.98	18.97	-0.47	0.22
	Temperate			-18.48	38.15	-0.56	0.19
	Continental			-28.23	12.5	-1.77	0.51
	Polar			-6.42	7.3	-0.39	0.517
IPSL-CM6A-LR	Global	-11.85	0	-8.76	5.74	-0.02	0.32
	Tropical	-30.01	0	-40.37	24.37	0.12	0.24
	Dry	-5.04	0	-7.23	16.74	-0.02	0.3
	Temperate	-16.28	0	-14.96	18.88	0	0.25
	Continental	-9.85	0	-7.77	10.16	-0.17	0.58
	Polar	-0.44	0	1.78	6.19	0.03	0.55
MIROC-ES2L	Global			0.85	12.43	0.03	0.24
	Tropical			1.78	70.37	-0.06	0.46

	Dry			-0.12	27.7	-0.01	0.34
	Temperate			0.95	34.91	0.01	0.22
	Continental			0.86	19.39	0.06	0.43
	Polar			0.97	6.33	0.07	0.36
UKESM1-0-L	Global	-10.63	0.77	-31.53	11.73	-0.93	0.31
	Tropical	-24.67	1.42	-92.9	69.8	-0.43	0.27
	Dry	-3.21	0.25	-5.17	18.64	-0.69	0.25
	Temperate	-19.25	1.34	-41.81	34.84	-0.75	0.27
	Continental	-21.43	1.73	-43.81	20.15	-2.17	0.74
	Polar	-0.89	0.07	-13.63	6.53	-0.53	0.56
MME	Global	-10.23	0.054	-10.15	3.24	-0.47	0.1
	Tropical	-27.49	0.164	-30.21	16.82	-0.12	0.11
	Dry	-2	0.142	-1.64	6.98	-0.32	0.1
	Temperate	-16.56	0.127	-11.6	9.52	-0.36	0.07
	Continental	-16.24	0.086	-13.07	5.55	-1.08	0.18
	Polar	-0.33	0.001	-5.42	2.59	-0.32	0.18

Table S4. Mean and standard deviation (SD) of Standardized Precipitation-Evapotranspiration Index (SPEI) annual changes for SPEI03, SPEI06, SPEI12, and SPEI24 in the later 30 years based on 9 LUMIP models (BCC-CSM2-MR, CMCC-ESM2, CNRM-ESM2-1, CanESM5, EC- Earth3-Veg, GISS-E2-1-G, IPSL-CM6A-LR, MIROC-ES2L, and UKESM1-0-LL) and multi-model ensemble (MME) results.

		SPEI03		SPEI06		SPEI12		SPEI24	
		Mean	SD	Mean	SD	Mean	SD	Mean	SD
BCC-CSM2-MR	Global	-0.04	0.05	-0.05	0.07	-0.07	0.08	-0.09	0.09
	Tropical	-0.16	0.1	-0.15	0.12	-0.16	0.15	-0.22	0.15
	Dry	0	0.11	0	0.14	0	0.17	0	0.18
	Temperate	-0.02	0.09	-0.02	0.11	-0.03	0.13	-0.04	0.14
	Continental	0	0.08	0.01	0.1	0.01	0.1	0	0.11
	Polar	-0.06	0.14	-0.09	0.19	-0.12	0.22	-0.16	0.25
CMCC-ESM2	Global	0.03	0.06	0.03	0.08	0.03	0.09	0.04	0.08
	Tropical	0.06	0.16	0.07	0.2	0.08	0.26	0.1	0.28
	Dry	0.12	0.13	0.24	0.18	0.16	0.18	0.22	0.18
	Temperate	0.03	0.09	0.03	0.12	0.02	0.16	0.03	0.17
	Continental	0.06	0.09	0.1	0.11	0.16	0.14	0.22	0.16
	Polar	-0.05	0.12	-0.08	0.15	-0.11	0.18	-0.16	0.17
CNRM-ESM2-1	Global	-0.01	0.05	-0.01	0.07	0	0.08	-0.01	0.09
	Tropical	-0.17	0.12	-0.2	0.15	-0.26	0.19	-0.37	0.21
	Dry	0.11	0.14	0.14	0.18	0.19	0.2	0.27	0.21
	Temperate	0.03	0.1	0.04	0.14	0.07	0.15	0.1	0.13
	Continental	0.08	0.06	0.13	0.08	0.2	0.09	0.28	0.1
	Polar	-0.08	0.1	-0.11	0.12	-0.14	0.15	-0.21	0.16
CanESM5	Global	-0.15	0.07	-0.17	0.09	-0.19	0.12	-0.25	0.13
	Tropical	-0.31	0.24	-0.32	0.28	-0.38	0.35	-0.52	0.38
	Dry	0.13	0.18	0.18	0.23	0.25	0.27	0.34	0.31
	Temperate	-0.12	0.12	-0.13	0.15	-0.15	0.17	-0.21	0.18
	Continental	-0.13	0.1	-0.13	0.13	-0.13	0.15	-0.17	0.19
	Polar	-0.25	0.15	-0.3	0.2	-0.38	0.25	-0.5	0.26
EC-Earth3-Veg	Global	0.03	0.05	0.04	0.07	0.04	0.09	0.06	0.09
	Tropical	0.04	0.1	0.04	0.12	0.03	0.14	0.05	0.15
	Dry	0.2	0.13	0.25	0.16	0.3	0.16	0.4	0.17
	Temperate	0.09	0.09	0.11	0.12	0.14	0.14	0.19	0.16

	Continental	-0.04	0.08	-0.05	0.09	-0.05	0.1	-0.07	0.11
	Polar	-0.01	0.12	-0.02	0.16	-0.04	0.2	-0.05	0.23
GISS-E2-1-G	Global	-0.29	0.14	-0.3	0.18	-0.31	0.21	-0.38	0.23
	Tropical	-0.6	0.27	-0.72	0.34	-0.91	0.47	-1.2	0.5
	Dry	-0.22	0.4	-0.21	0.51	-0.19	0.6	-0.21	0.7
	Temperate	-0.19	0.3	-0.18	0.37	-0.18	0.43	-0.22	0.48
	Continental	-0.33	0.2	-0.37	0.26	-0.41	0.26	-0.56	0.27
	Polar	-0.22	0.25	-0.19	0.33	-0.15	0.42	-0.12	0.43
IPSL-CM6A-LR	Global	-0.05	0.04	-0.07	0.06	-0.11	0.07	-0.15	0.08
	Tropical	-0.37	0.07	-0.46	0.09	-0.62	0.11	-0.86	0.1
	Dry	0.04	0.12	0.06	0.16	0.07	0.17	0.07	0.14
	Temperate	-0.09	0.06	-0.12	0.08	-0.17	0.1	-0.24	0.11
	Continental	-0.05	0.05	-0.08	0.07	-0.11	0.08	-0.16	0.09
	Polar	0.02	0.09	0.01	0.12	0.01	0.17	0	0.19
MIROC-ES2L	Global	0.02	0.06	0.03	0.07	0.03	0.1	0.04	0.12
	Tropical	0.03	0.16	0.04	0.2	0.06	0.25	0.09	0.27
	Dry	-0.01	0.17	-0.01	0.22	-0.01	0.28	-0.01	0.34
	Temperate	-0.01	0.11	-0.02	0.14	-0.02	0.18	-0.02	0.2
	Continental	-0.01	0.1	-0.01	0.12	-0.02	0.12	-0.04	0.14
	Polar	0.05	0.1	0.07	0.12	0.08	0.15	0.11	0.16
UKESM1-0-L	Global	-0.06	0.04	-0.08	0.05	-0.11	0.06	-0.17	0.06
	Tropical	-0.21	0.15	-0.29	0.18	-0.39	0.24	-0.54	0.3
	Dry	0.28	0.13	0.36	0.16	0.48	0.2	0.65	0.2
	Temperate	-0.02	0.08	-0.03	0.1	-0.05	0.12	-0.06	0.13
	Continental	-0.1	0.07	-0.13	0.09	-0.16	0.1	-0.23	0.1
	Polar	-0.14	0.1	-0.2	0.14	-0.27	0.15	-0.4	0.16
MME	Global	-0.06	0.02	-0.06	0.03	-0.08	0.03	-0.1	0.03
	Tropical	-0.19	0.04	-0.22	0.05	-0.28	0.07	-0.39	0.07
	Dry	0.07	0.05	0.1	0.07	0.14	0.08	0.19	0.08
	Temperate	-0.03	0.04	-0.04	0.05	-0.04	0.06	-0.05	0.06
	Continental	-0.06	0.03	-0.06	0.04	-0.06	0.04	-0.08	0.04
	Polar	-0.08	0.04	-0.1	0.06	-0.12	0.07	-0.16	0.08

Table S5. Mean and standard deviation (SD) of the seasonal mean (DJF: December-January-February; MAM: March-April-May; JJA: June- July-August; SON: September-October-November) changes in the SPEI03 over the latter 30 years of deforestation simulations, based on results from nine LUMIP models (BCC-CSM2-MR, CMCC-ESM2, CNRM-ESM2-1, CanESM5, EC-Earth3-Veg, GISS-E2-1-G, IPSL-CM6A-LR, MIROC-ES2L, and UKESM1-0-LL), as well as the multi-model ensemble (MME) results.

		SPEI03		SPEI06		SPEI12		SPEI24	
		Mean	SD	Mean	SD	Mean	SD	Mean	SD
BCC-CSM2-MR	Global	-0.04	0.1	-0.05	0.07	-0.03	0.08	-0.06	0.1
	Tropical	-0.13	0.16	-0.16	0.19	-0.14	0.15	-0.26	0.18
	Dry_n	-0.01	0.32	0	0.28	-0.01	0.18	-0.01	0.32
	Dry_s	0.1	0.28	0.01	0.27	-0.03	0.2	0.01	0.37
	T_n	-0.05	0.23	-0.06	0.2	0.04	0.17	0.02	0.2
	T_s	0	0.21	-0.03	0.24	-0.15	0.22	-0.03	0.27
	CONT	-0.06	0.17	0.09	0.15	0.03	0.12	-0.04	0.11
	Polar_n	0	0.17	-0.09	0.24	-0.01	0.21	-0.06	0.21
	Polar_s	-0.03	0.28	-0.12	0.22	-0.06	0.27	-0.05	0.28
CMCC-ESM2	Global	-0.03	0.08	0.04	0.11	0.06	0.08	0.03	0.09
	Tropical	0.03	0.2	0.08	0.17	0.08	0.2	0.05	0.26
	Dry_n	0.14	0.33	0.09	0.35	0.1	0.37	0.19	0.24

	Dry_s	0.09	0.47	0.16	0.49	0.1	0.45	0.19	0.44
	T_n	0.02	0.17	0.01	0.17	0.03	0.2	0.05	0.18
	T_s	-0.02	0.19	0.04	0.21	0.02	0.23	0.11	0.2
	CONT	-0.15	0.17	0.12	0.15	0.23	0.13	0.05	0.14
	Polar_n	-0.16	0.23	-0.1	0.21	0.03	0.21	-0.16	0.23
	Polar_s	-0.02	0.24	-0.02	0.23	-0.08	0.22	-0.02	0.27
CNRM-ESM2-1	Global	-0.06	0.1	0	0.08	0.07	0.07	-0.04	0.08
	Tropical	-0.17	0.19	-0.08	0.17	-0.09	0.19	-0.36	0.19
	Dry_n	0.01	0.25	0.12	0.29	0.2	0.3	0.17	0.27
	Dry_s	0.01	0.35	0.19	0.26	0.12	0.29	-0.03	0.29
	T_n	0.01	0.23	-0.05	0.2	0.17	0.12	0.1	0.13
	T_s	0.01	0.2	-0.07	0.23	-0.06	0.23	-0.08	0.23
	CONT	-0.05	0.14	0.07	0.14	0.24	0.1	0.07	0.09
	Polar_n	-0.19	0.19	-0.1	0.24	0.03	0.19	-0.09	0.18
	Polar_s	-0.07	0.28	-0.05	0.2	-0.08	0.18	-0.1	0.24
CanESM5	Global	-0.23	0.13	-0.14	0.11	-0.08	0.08	-0.17	0.1
	Tropical	-0.34	0.37	-0.29	0.24	-0.25	0.26	-0.37	0.38
	Dry_n	0.15	0.33	0.14	0.34	0.2	0.4	0.31	0.32
	Dry_s	-0.09	0.48	-0.1	0.47	-0.11	0.56	0.05	0.48
	T_n	-0.19	0.29	-0.08	0.15	-0.07	0.22	-0.13	0.25
	T_s	-0.03	0.22	-0.15	0.21	-0.23	0.27	-0.07	0.35
	CONT	-0.41	0.22	-0.01	0.15	0.17	0.13	-0.28	0.14
	Polar_n	-0.45	0.29	-0.32	0.27	-0.11	0.28	-0.35	0.17
	Polar_s	-0.19	0.39	-0.25	0.33	-0.3	0.28	-0.19	0.34
EC-Earth3-Veg	Global	-0.01	0.08	0.02	0.09	0.06	0.1	0.07	0.08
	Tropical	0.07	0.12	0.08	0.18	-0.03	0.15	0.03	0.17
	Dry_n	0.2	0.31	0.25	0.36	0.27	0.26	0.32	0.22
	Dry_s	-0.04	0.28	-0.09	0.41	0.07	0.39	0.17	0.35
	T_n	0.06	0.19	0.07	0.16	0.22	0.16	0.14	0.11
	T_s	0.06	0.16	-0.07	0.27	-0.03	0.22	0.04	0.2
	CONT	-0.16	0.16	-0.02	0.16	0.05	0.09	-0.04	0.13
	Polar_n	-0.06	0.21	-0.07	0.23	-0.09	0.23	-0.1	0.19
	Polar_s	-0.01	0.26	-0.03	0.27	0.3	0.26	0.09	0.24
GISS-E2-1-G	Global	-0.38	0.24	-0.31	0.22	-0.21	0.25	-0.29	0.17
	Tropical	-0.59	0.36	-0.56	0.36	-0.69	0.5	-0.61	0.41
	Dry_n	-0.1	0.52	-0.44	0.76	-0.27	0.93	0.1	0.61
	Dry_s	-0.26	0.63	-0.44	0.64	-0.47	0.69	-0.28	0.6
	T_n	-0.21	0.48	-0.21	0.42	-0.21	0.41	-0.15	0.37
	T_s	-0.15	0.33	-0.17	0.5	-0.3	0.55	-0.13	0.46
	CONT	-0.75	0.41	-0.24	0.38	0.09	0.33	-0.46	0.26
	Polar_n	-0.69	0.56	-0.55	0.41	0.08	0.42	-0.43	0.36
	Polar_s	-0.07	0.58	-0.13	0.52	-0.26	0.6	-0.18	0.54
IPSL-CM6A-LR	Global	-0.06	0.09	-0.04	0.08	-0.05	0.06	-0.08	0.07
	Tropical	-0.34	0.12	-0.29	0.11	-0.4	0.1	-0.45	0.19
	Dry_n	0	0.24	0.01	0.29	0.05	0.26	0.01	0.25
	Dry_s	0.04	0.4	-0.03	0.32	-0.28	0.37	-0.05	0.38
	T_n	-0.07	0.2	-0.03	0.13	-0.01	0.13	-0.05	0.14
	T_s	-0.17	0.27	-0.21	0.21	-0.32	0.19	-0.17	0.23
	CONT	0	0.14	-0.05	0.09	-0.06	0.11	-0.08	0.09
	Polar_n	0.01	0.16	0.05	0.24	0.07	0.15	0.02	0.13
	Polar_s	-0.03	0.3	0	0.24	-0.03	0.22	-0.03	0.22
MIROC-ES2L	Global	0.02	0.1	0.02	0.07	0.04	0.06	0	0.1
	Tropical	0.03	0.15	0.03	0.15	0.03	0.2	0.02	0.29
	Dry_n	-0.02	0.32	-0.01	0.33	0.03	0.34	-0.02	0.32
	Dry_s	-0.01	0.38	0.01	0.32	0.08	0.35	-0.1	0.37

	T_n	0.06	0.25	-0.01	0.23	-0.01	0.18	-0.04	0.2
	T_s	0	0.27	-0.07	0.27	-0.01	0.25	-0.06	0.21
	CONT	-0.04	0.17	0.01	0.2	0.01	0.1	-0.03	0.1
	Polar_n	0.05	0.18	0.07	0.24	0.02	0.25	-0.01	0.16
	Polar_s	0.06	0.27	0.02	0.2	0.09	0.17	0.07	0.24
	Global	-0.1	0.08	-0.04	0.08	-0.03	0.07	-0.06	0.08
	Tropical	-0.21	0.19	-0.19	0.22	-0.24	0.17	-0.21	0.23
	Dry_n	0.28	0.26	0.28	0.35	0.5	0.28	0.39	0.19
	Dry_s	0	0.36	0.01	0.37	0	0.4	0.11	0.34
UKESM1-0-LL	T_n	-0.07	0.16	0.02	0.2	0.14	0.17	0.06	0.11
	T_s	-0.06	0.26	-0.18	0.2	-0.26	0.21	-0.1	0.22
	CONT	-0.22	0.14	-0.08	0.14	-0.01	0.08	-0.1	0.09
	Polar_n	-0.28	0.19	-0.33	0.28	-0.24	0.17	-0.25	0.19
	Polar_s	-0.09	0.24	0.01	0.26	-0.13	0.26	-0.15	0.23
	Global	-0.1	0.04	-0.05	0.03	-0.02	0.04	-0.07	0.03
	Tropical	-0.18	0.07	-0.15	0.07	-0.19	0.08	-0.24	0.08
	Dry_n	0.08	0.13	0.06	0.1	0.13	0.14	0.17	0.11
	Dry_s	-0.01	0.15	-0.05	0.13	-0.06	0.14	-0.01	0.15
MME	T_n	-0.05	0.08	-0.03	0.07	0.03	0.06	0	0.07
	T_s	-0.04	0.09	-0.1	0.08	-0.15	0.09	-0.06	0.1
	CONT	-0.2	0.07	-0.01	0.07	0.08	0.04	-0.1	0.04
	Polar_n	-0.2	0.08	-0.15	0.11	-0.03	0.07	-0.16	0.07
	Polar_s	-0.05	0.1	-0.06	0.09	-0.08	0.11	-0.06	0.1

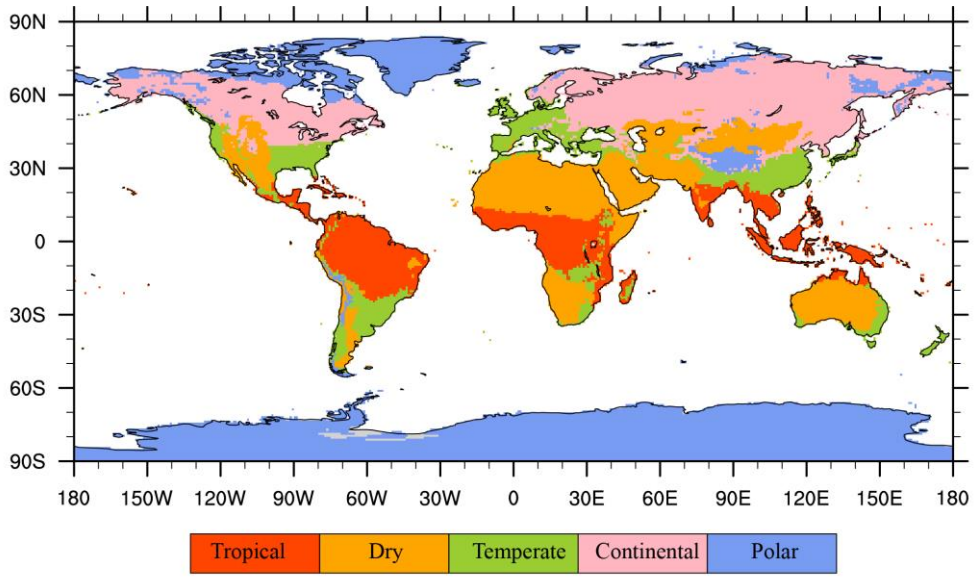

Figure S1. World map showing the main climate classifications according to the Köppen-Geiger system. The map displays the various climatic zones across the world, based on temperature and precipitation patterns. And the system classifies climates into five major groups: Tropical, Dry, Temperate, Continental, and Polar.

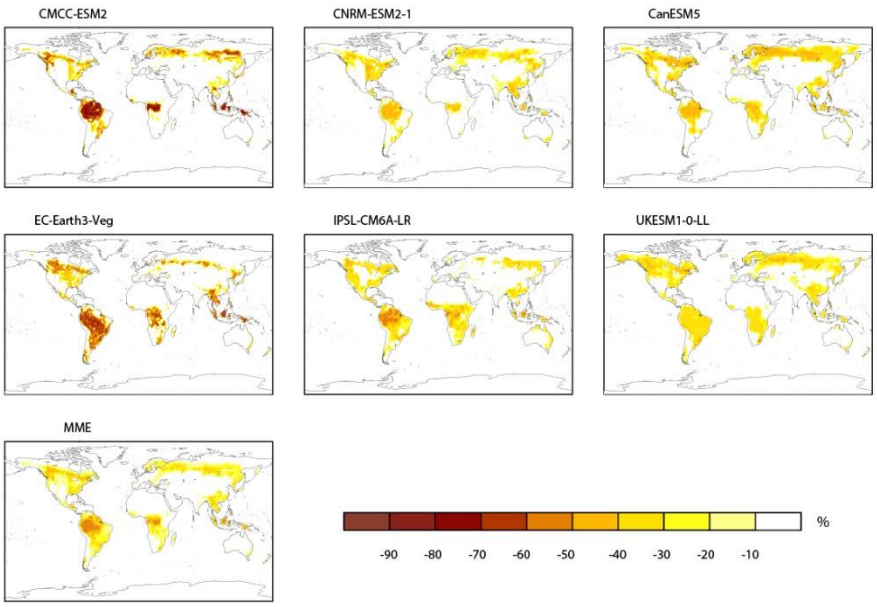

Figure S2. Global land-based forest fraction changes resulting from an idealized deforestation scenario (*deforest-global* minus *piControl*) for six climate models (CMCC-ESM2, CNRM-ESM2-1, CanESM5, EC-Earth3-Veg, IPSL-CM6A-LR, and UKESM1-0-LL), and their multi-model ensemble mean (MME). The six models were the only ones available to show the forest fraction changes at the time of the study.

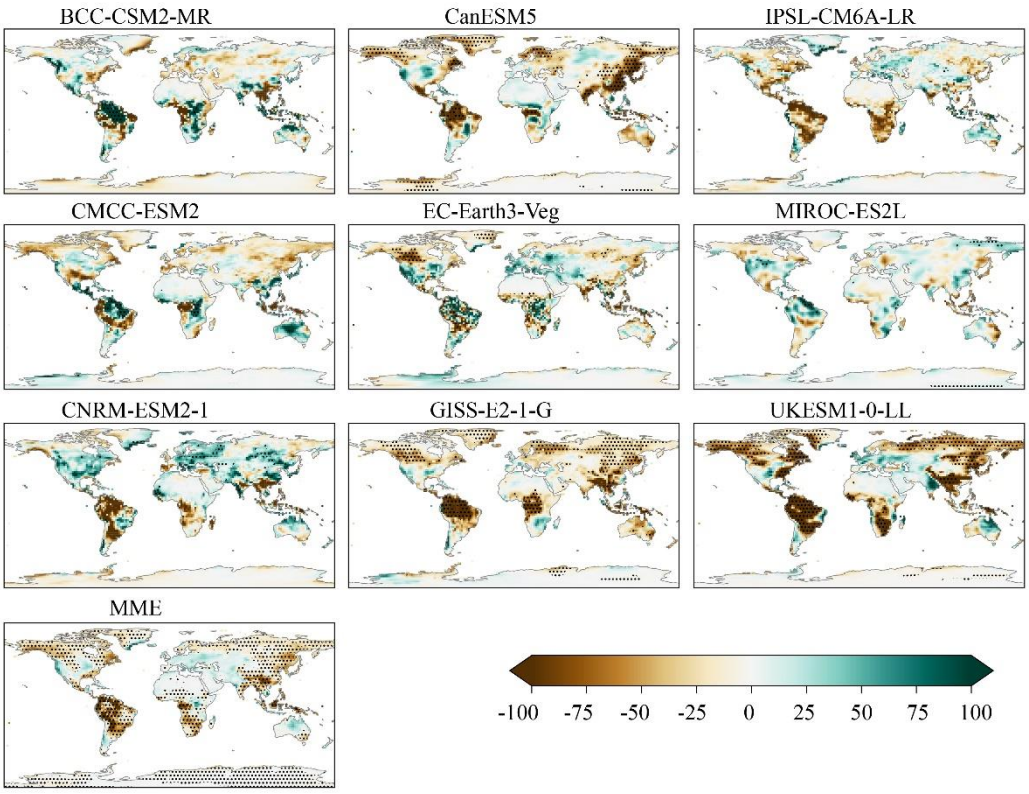

Figure S3. Global land-based precipitation changes (mm yr^{-1}) resulting from an idealized deforestation scenario (*deforest-global* minus *piControl*) for nine climate models (BCC-CSM2-MR, CMCC-ESM2, CNRM-ESM2-1, CanESM5, EC-Earth3-Veg, GISS-E2-1-G, IPSL-CM6A-LR, MIROC-ES2L, and UKESM1-0-LL), and their multi-model ensemble mean (MME) averaged for the last 30 years. The map shows the changes in the multi-year average of annual total precipitation, compared to *piControl* experiment. The black dots indicate the changes in precipitation, with significance tested using a two-tailed t-test at a p-value of 0.05.

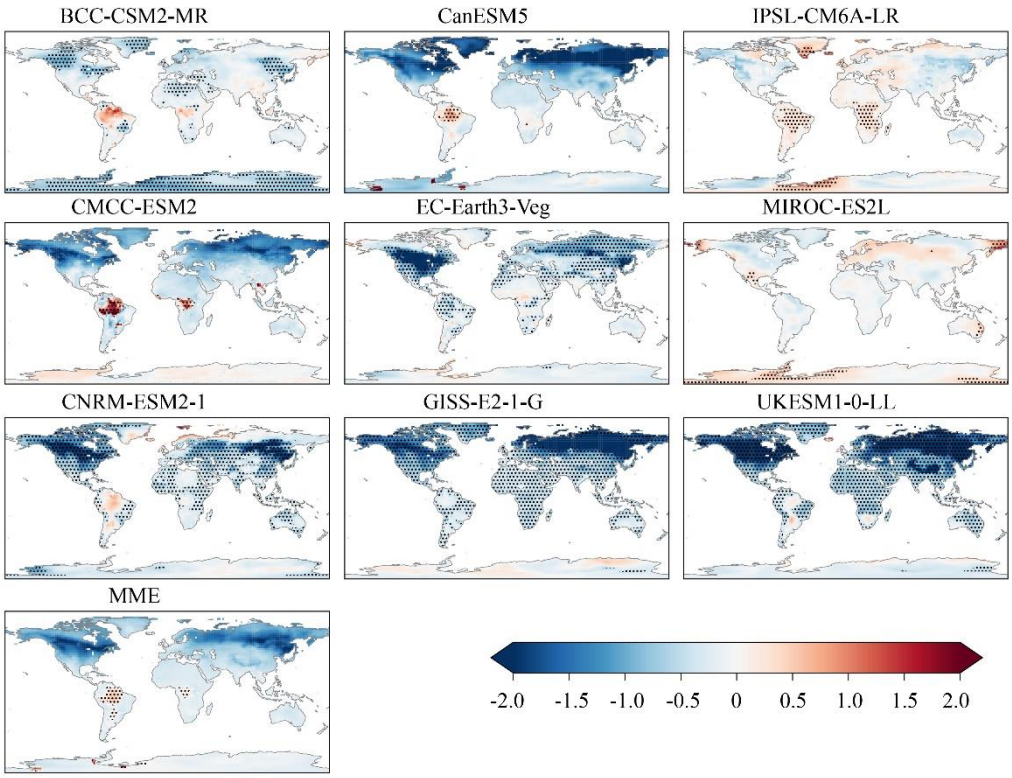

Figure S4. Global land-based temperature changes (°C) resulting from an idealized deforestation scenario (*deforest-global* minus *piControl*) for nine climate models (BCC-CSM2-MR, CMCC-ESM2, CNRM-ESM2-1, CanESM5, EC-Earth3-Veg, GISS-E2-1-G, IPSL-CM6A-LR, MIROC-ES2L, and UKESM1-0-LL), and their multi-model ensemble mean (MME) averaged for the last 30 years. The map shows the changes in the multi-year average of annual mean temperature, compared to *piControl* experiment. The black dots indicate the changes in temperature, with significance tested using a two-tailed t-test at a p-value of 0.05.

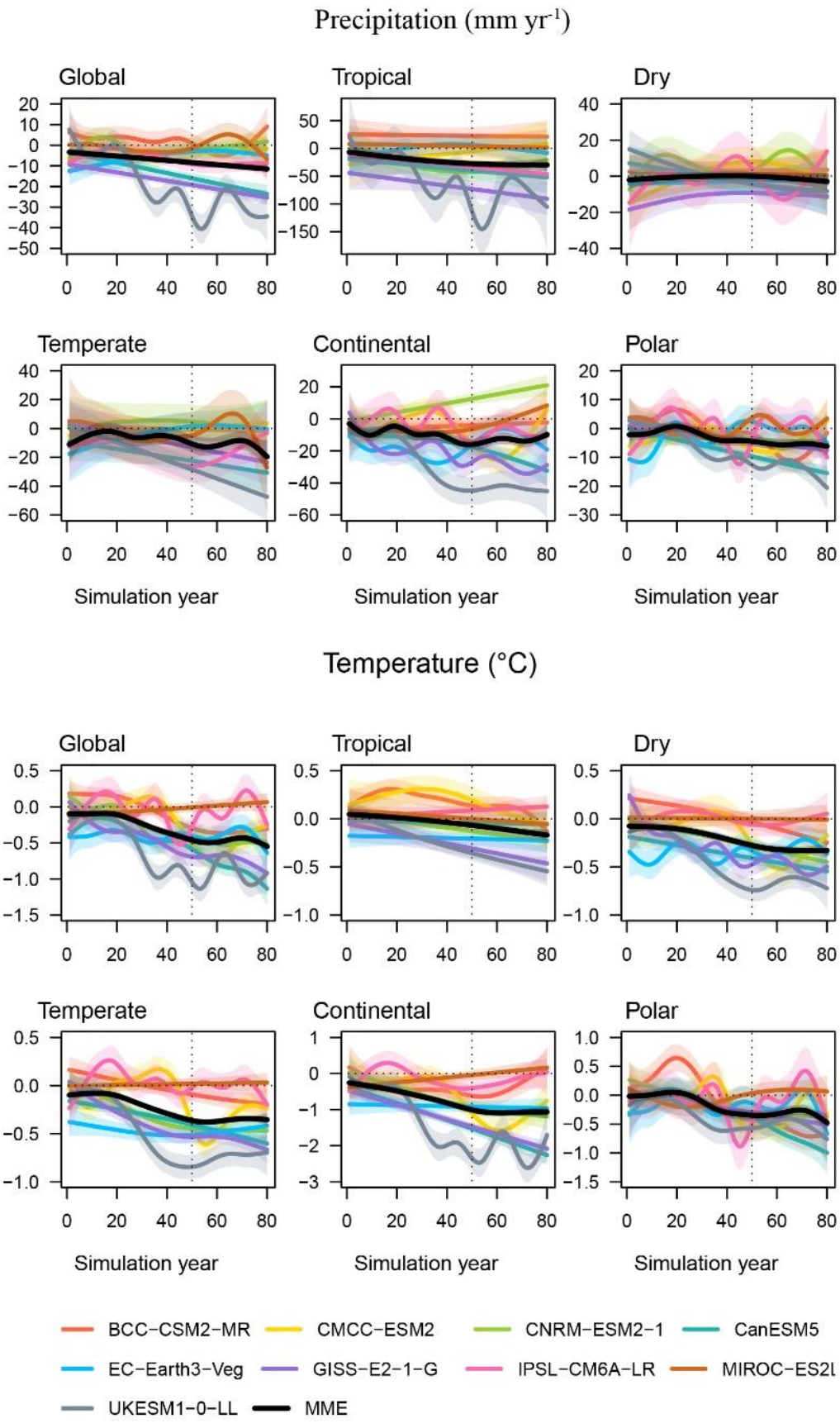

Figure S5. The time series of precipitation and near surface air temperature changes resulting from idealized deforestation, globally (land areas only) and climate zonally averaged, for each model and MME. The colors represent different models, and the information is provided at the bottom of the figure. The solid lines indicate cubic spline regression results, and the colored areas denote the range of significance level of 0.05.

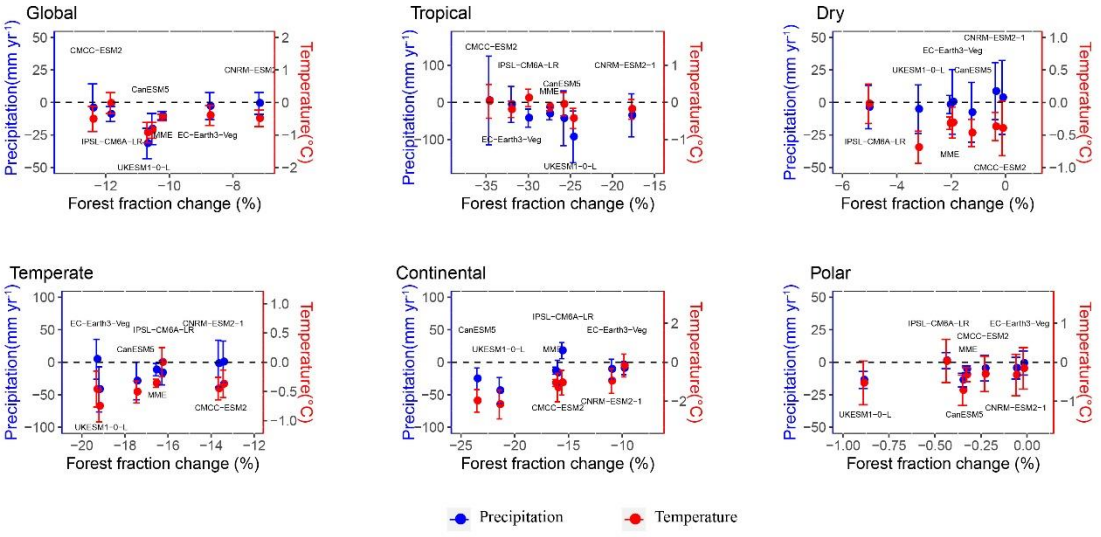

Figure S6. Global and regional mean changes in forest fraction (%), precipitation (mm yr^{-1}), and near-surface air temperature (°C). The data points represent the 30-year average (from simulation year 51 to 80) of individual model outcomes, while the vertical error bars indicate the range of results derived from the land grid cells.

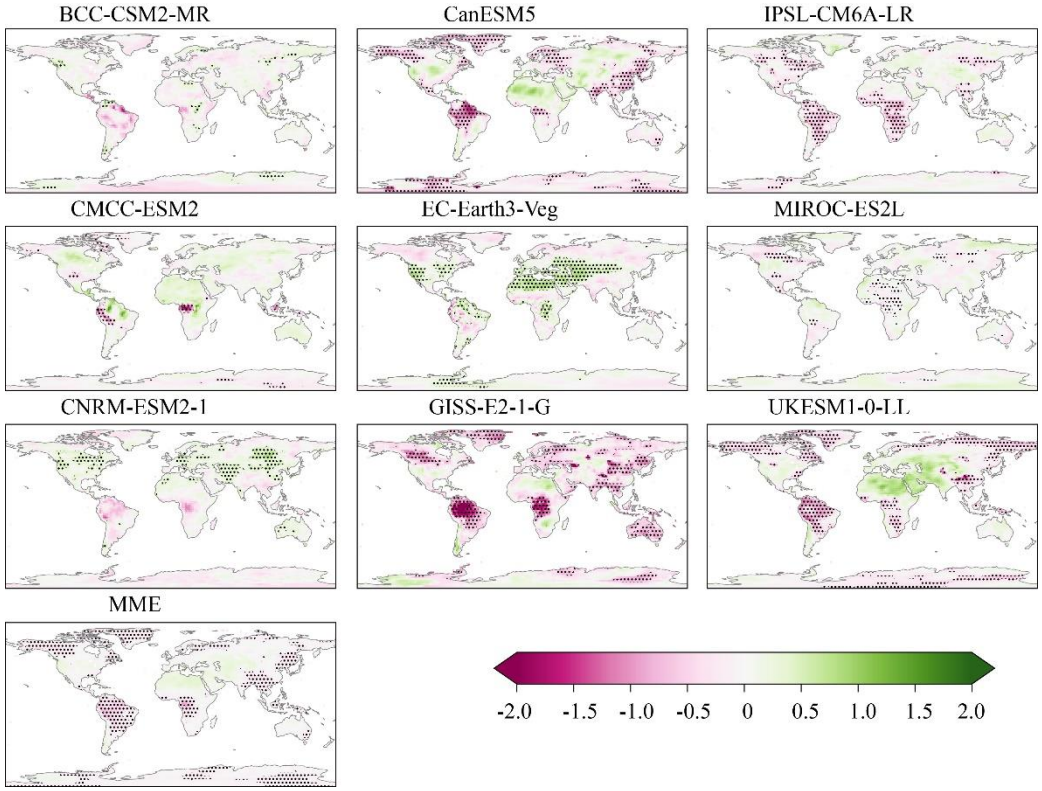

Figure S7. Changes in mid-term Standardized Precipitation-Evapotranspiration Index (SPEI06) averaged from year 51 to 80 for each model and the multi-model ensemble mean (MME). The map shows in the multi-year average of annual averaged SPEI06 calculated from *deforest-global* experiment, and the reference period is from *piControl* experiment. The black dots indicate the changes in SPEI06, with significance tested using a two-tailed t-test at a p-value of 0.05.

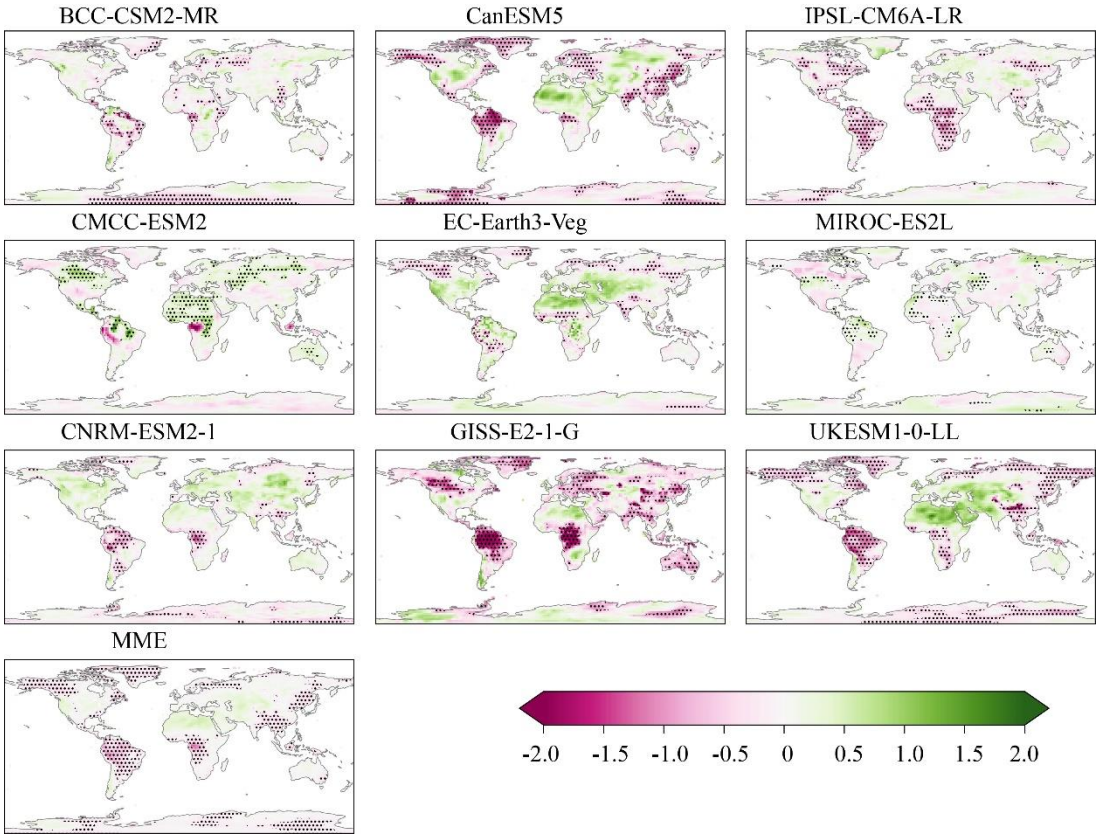

Figure S8. Changes in mid-term Standardized Precipitation-Evapotranspiration Index (SPEI12) averaged from year 51 to 80 for each model and the multi-model ensemble mean (MME). The map shows in the multi-year average of annual averaged SPEI12 calculated from *deforest-global* experiment, and the reference period is from *piControl* experiment. The black dots indicate the changes in SPEI03, with significance tested using a two-tailed t-test at a p-value of 0.05.

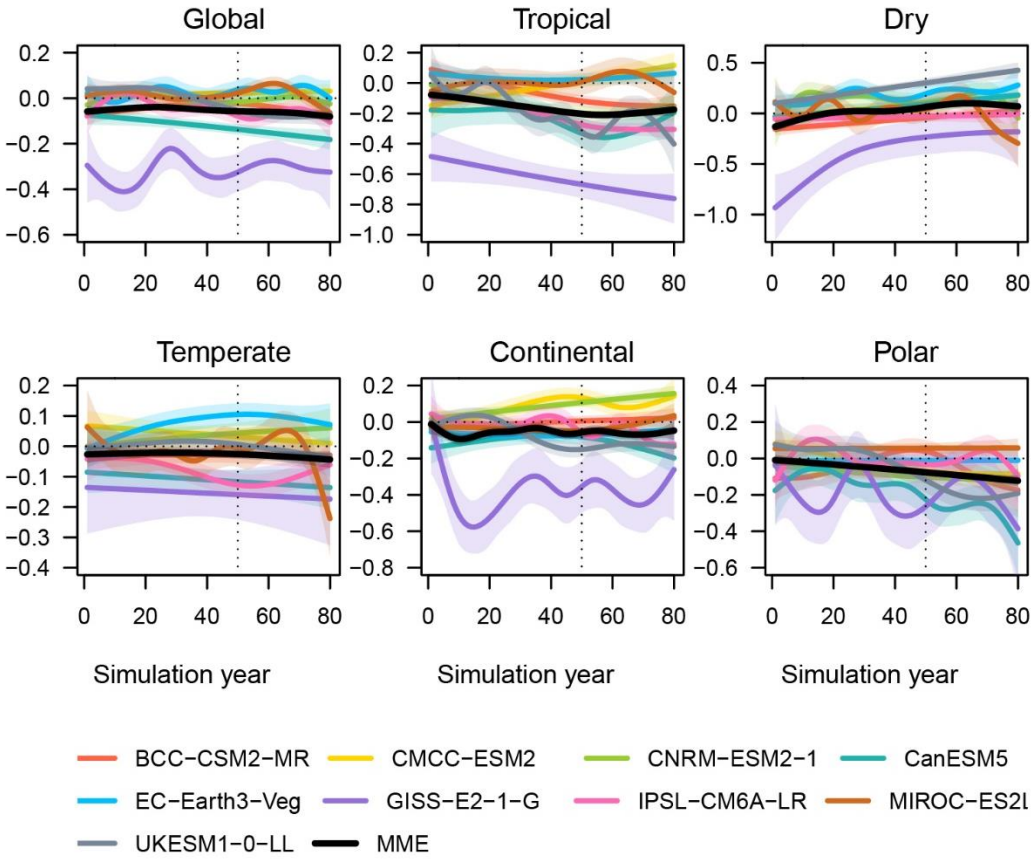

Figure S9. Time series analysis of globally and zonally averaged Standardized Precipitation-Evapotranspiration Index (SPEI06) change (calculated from *deforest-global* experiment, and the reference period is from *piControl* experiment) for each model and multi-model ensemble (MME). The data points correspond to the model output, and the solid lines represent the cubic spline regression line. The colored areas refer to the range of significance level of 0.05.

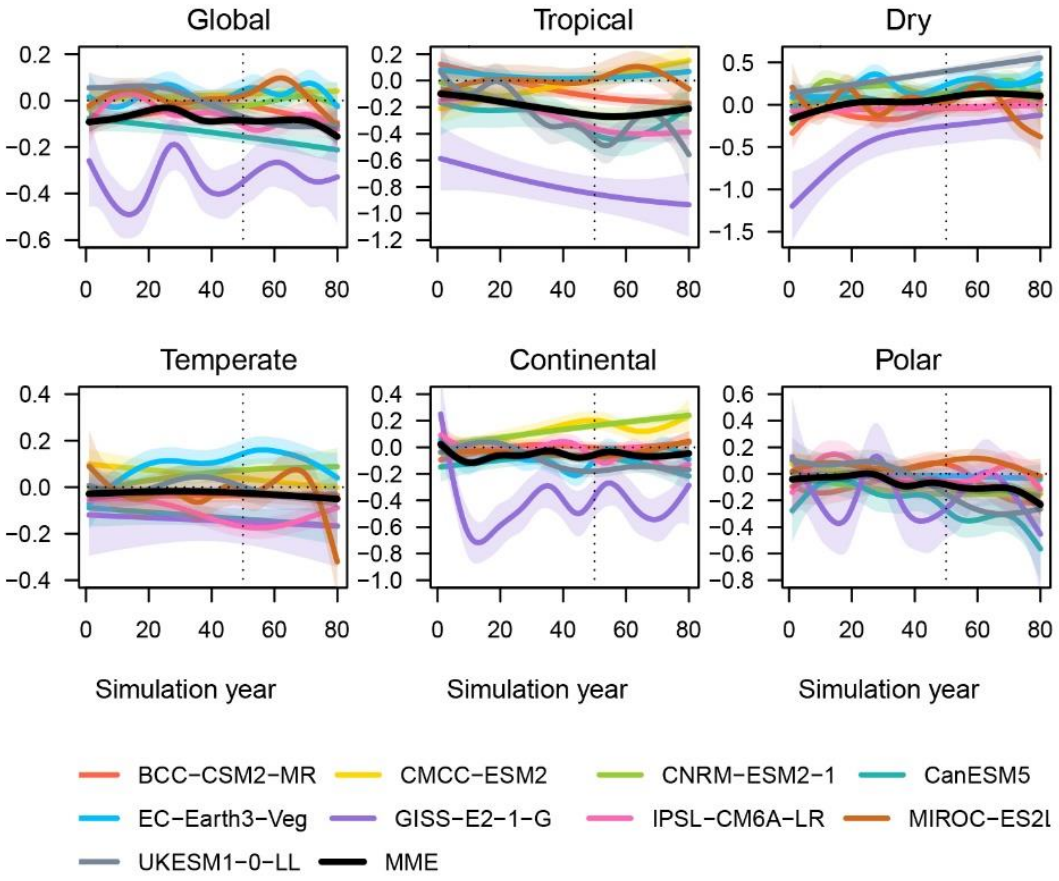

Figure S10. Time series analysis of globally and zonally averaged Standardized Precipitation-Evapotranspiration Index (SPEI12) change (calculated from *deforest-global* experiment, and the reference period is from *piControl* experiment) for each model and multi-model ensemble (MME). The data points correspond to the model output, and the solid lines represent the cubic spline regression line. The colored areas refer to the range of significance level of 0.05.

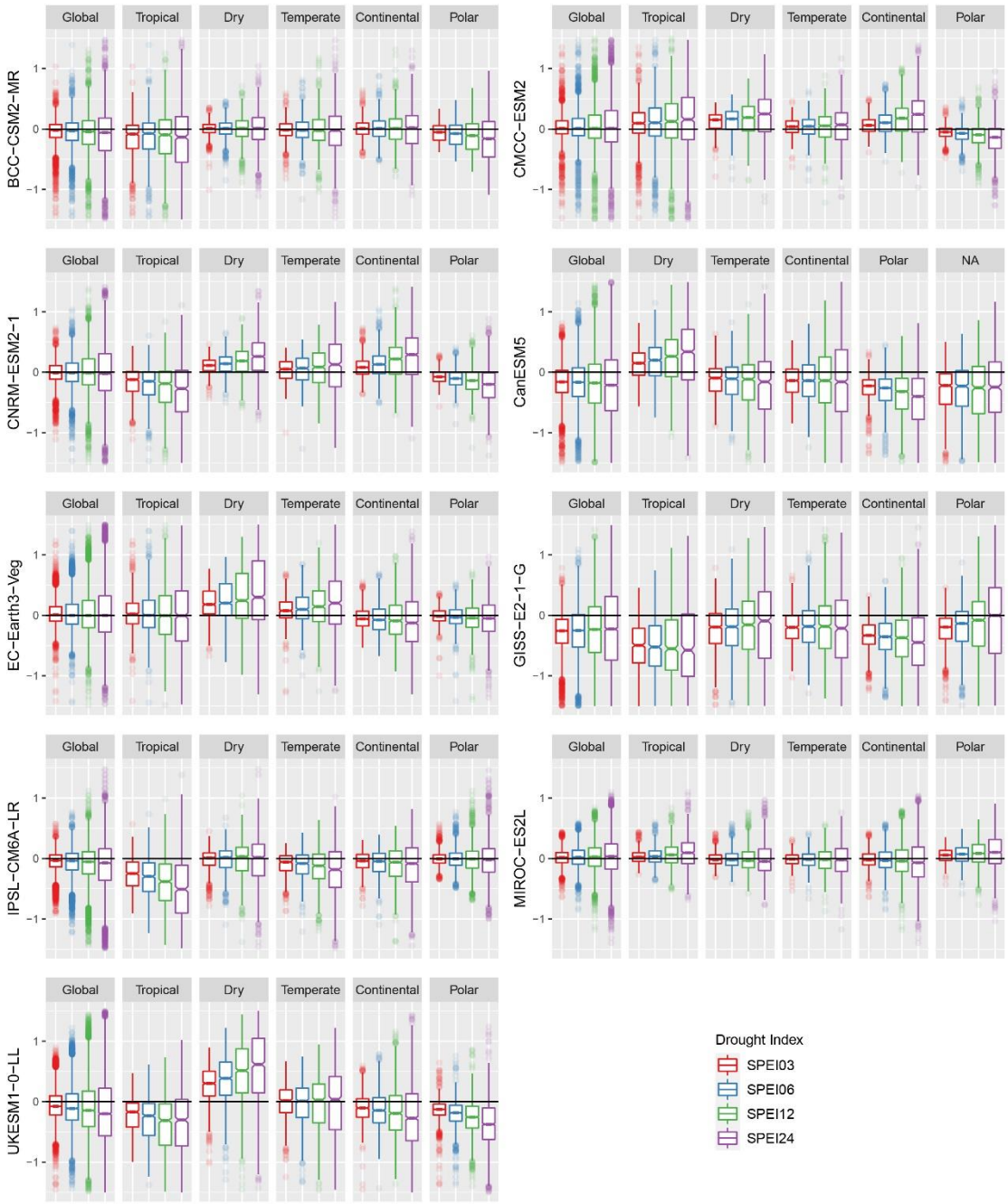

Figure S11. The box plots display the distribution of SPEIs (SPEI03, SPEI06, SPEI12, SPEI24) changes induced by deforestation averaged from year 51 to 80, globally and over the five climate regions for individual model. Each box plot represents the variability of a specific SPEI, where the box represents the interquartile range (IQR) between the 25th and 75th percentiles, and the line inside the box represents the median. The whiskers extend to the minimum and maximum values within 1.5 times the IQR, and any data beyond the whiskers are shown as points. Different colors indicate different SPEIs.

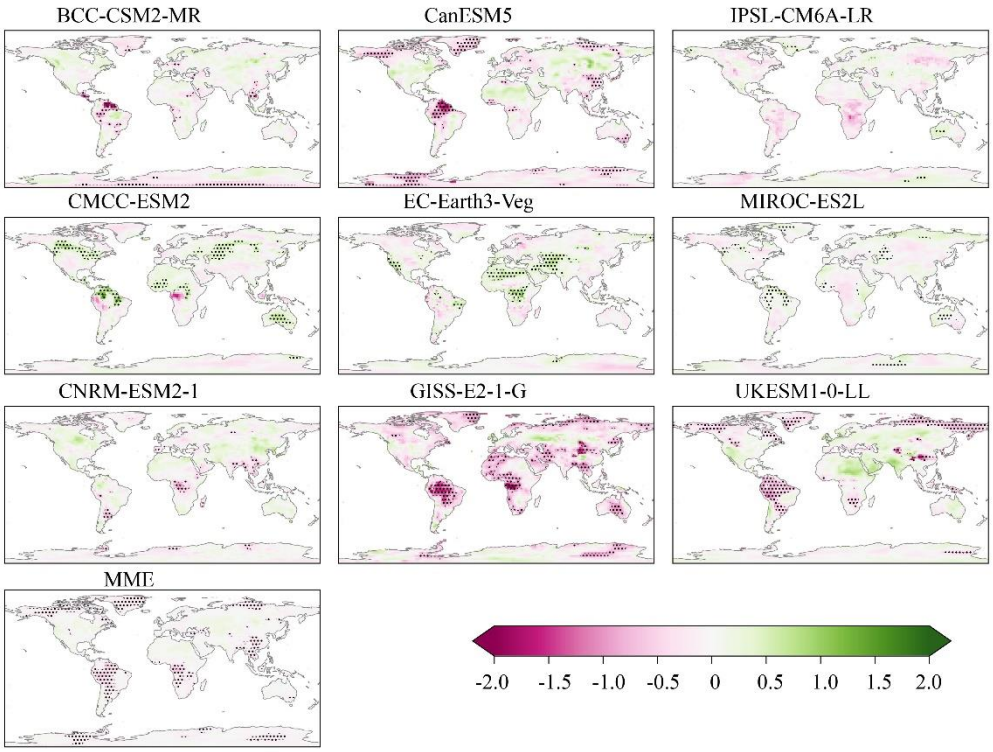

Figure S12. Maps of Standardized Precipitation-Evapotranspiration Index (SPEI03) change during March-April-May (MAM) season, averaged from year 51 to 80, for each individual model and the multi-model ensemble (MME) results. The map shows the changes in the multi-year average of seasonal averaged SPEI03, calculated from *deforest-global* experiment, and the reference period is from *piControl* experiment.

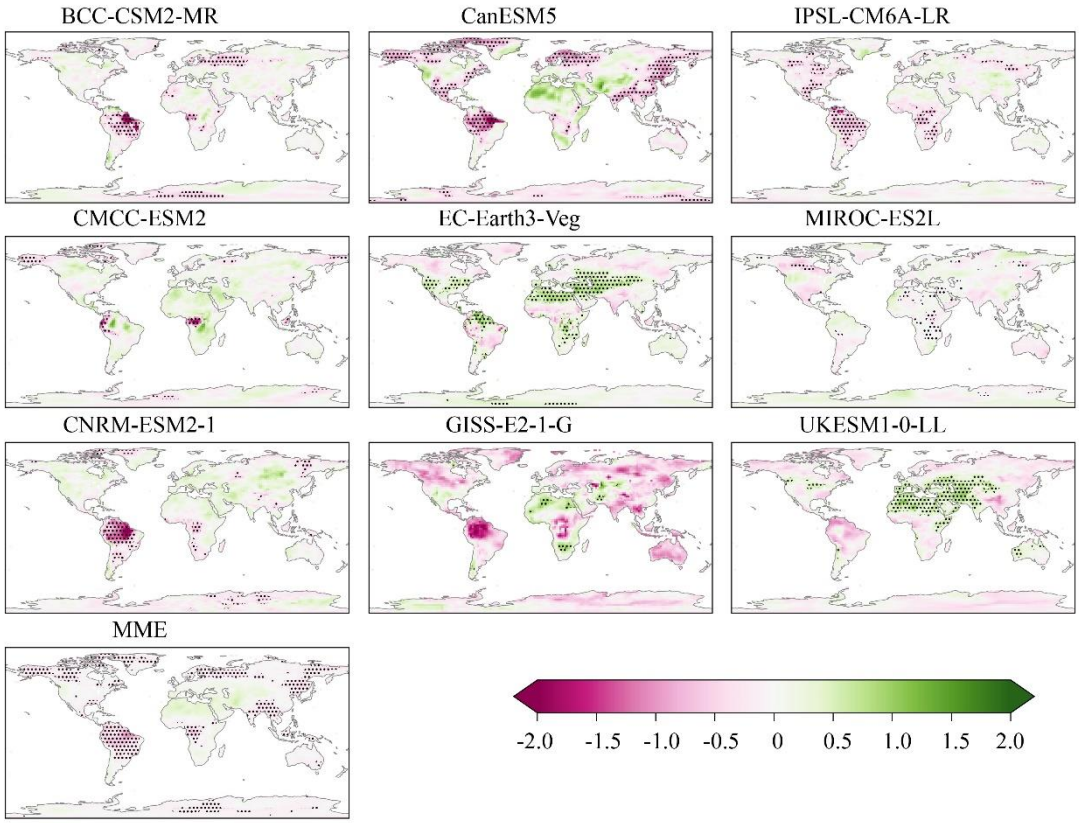

Figure S13. Maps of Standardized Precipitation-Evapotranspiration Index (SPEI03) change during September-October-November (SON) season, averaged from year 51 to 80, for each individual model and the multi-model ensemble (MME) results. The map shows the changes in the multi-year average of seasonal averaged SPEI03, calculated from *deforest-global* experiment, and the reference period is from *piControl* experiment.

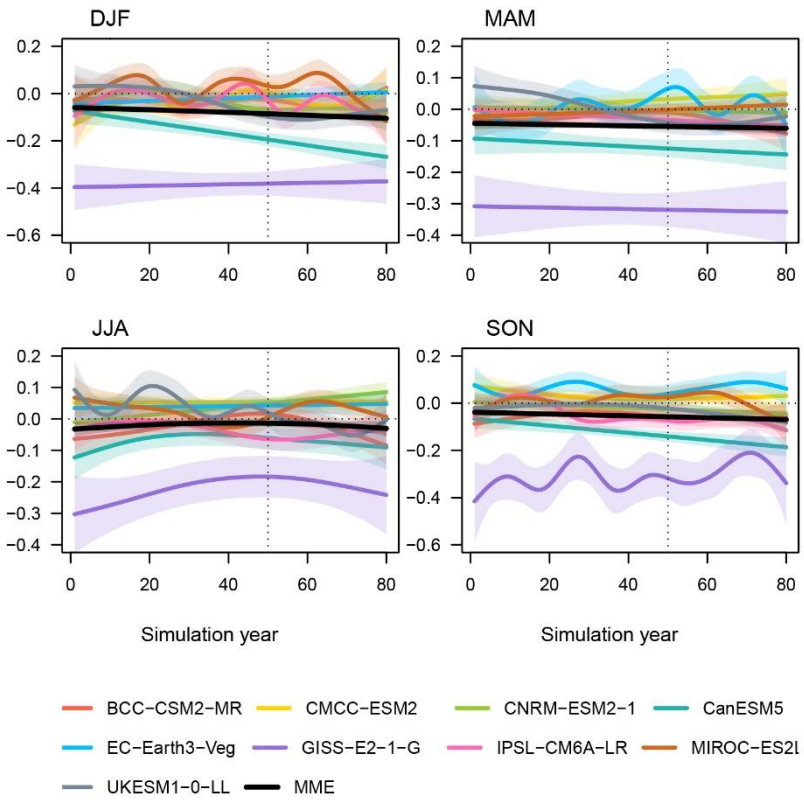

Figure S14. Seasonal time series of SPEI03 change averaged globally for each individual model and the MME, covering four seasons (DJF, MAM, JJA, SON). Different colors represent different models, and the information is provided at the bottom of the figure. The solid lines denote cubic spline regression, with significance indicated by colored areas at a level of 0.05.

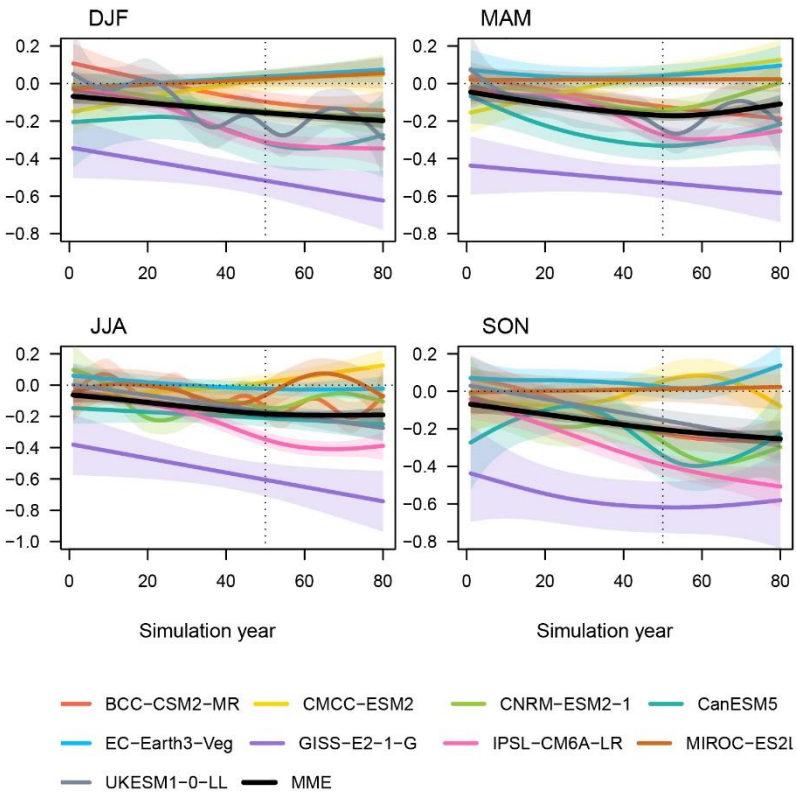

Figure S15. Seasonal time series of SPEI03 change averaged tropical region for each individual model and the MME, covering four seasons (DJF, MAM, JJA, SON). Different colors represent different models, and the information is provided at the bottom of the figure. The solid lines denote cubic spline regression, with significance indicated by colored areas at a level of 0.05.

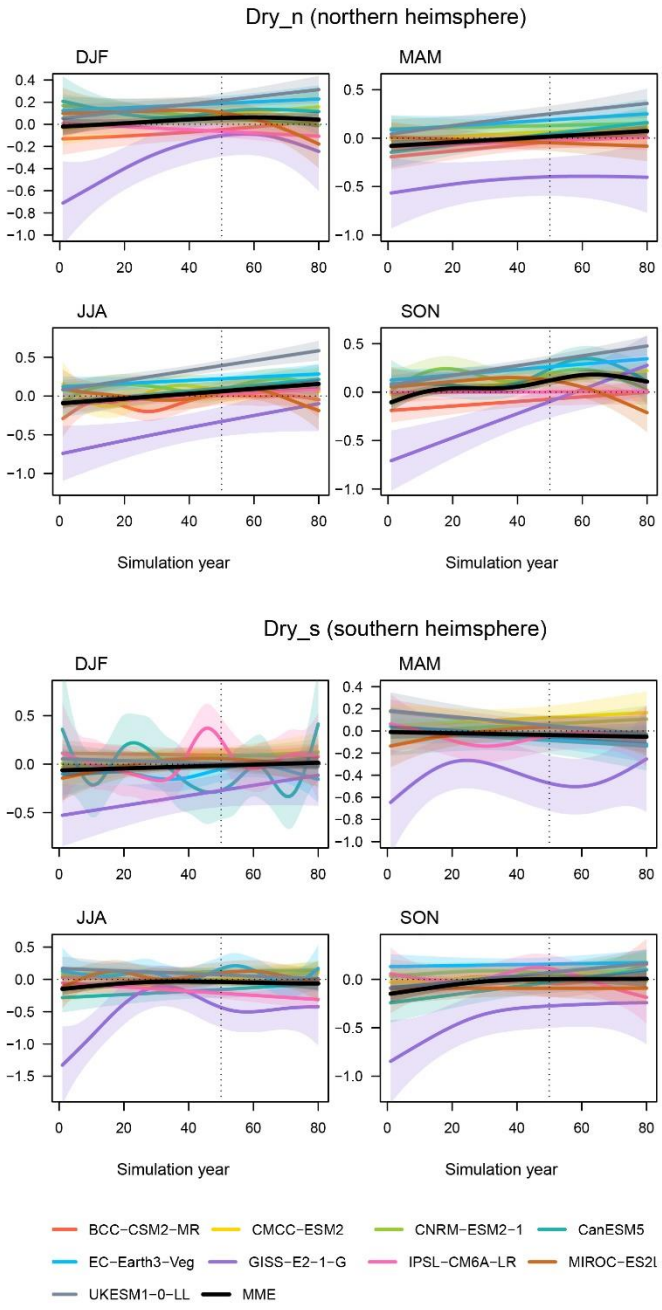

Figure S16. Seasonal changes in SPEI03 induced by deforestation averaged in the dry regions of the northern hemisphere (upper pane) and southern hemisphere (lower pane). The solid lines denote cubic spline regression, with significance indicated by colored areas at a level of 0.05.

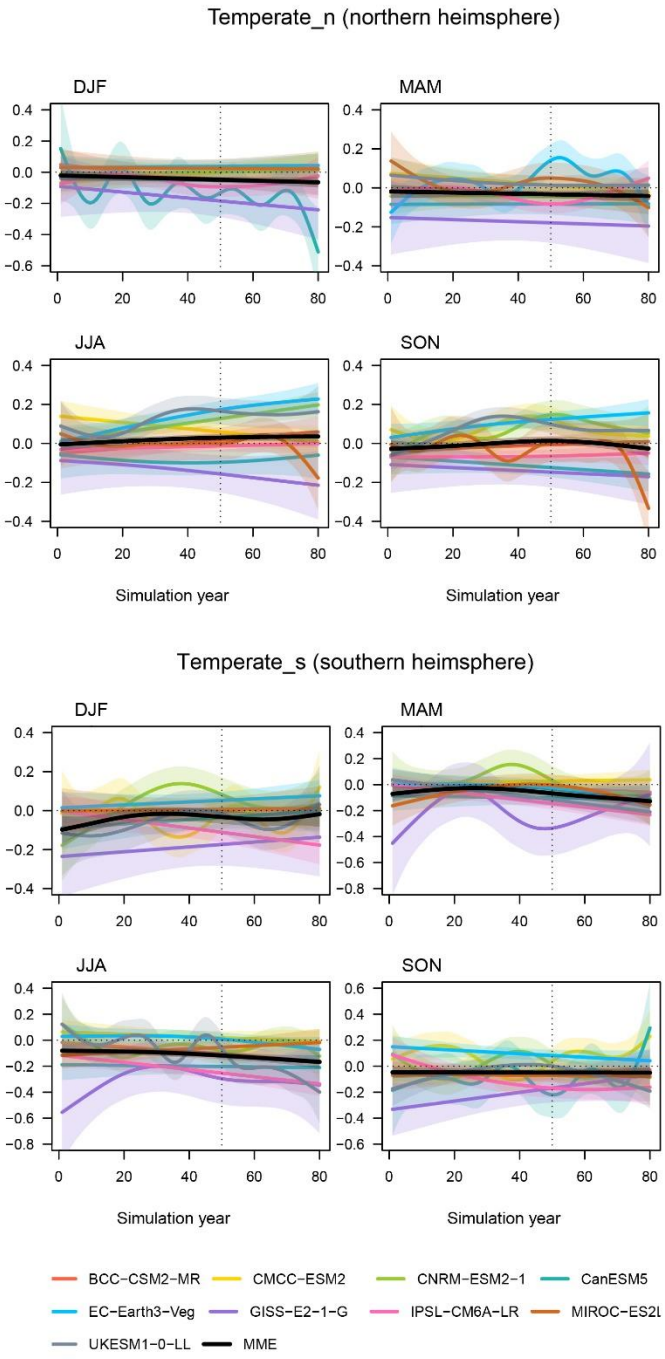

Figure S17. Seasonal changes in SPEI03 induced by deforestation averaged in the temperate regions of the northern hemisphere (upper pane) and southern hemisphere (lower pane). The solid lines denote cubic spline regression, with significance indicated by colored areas at a level of 0.05.

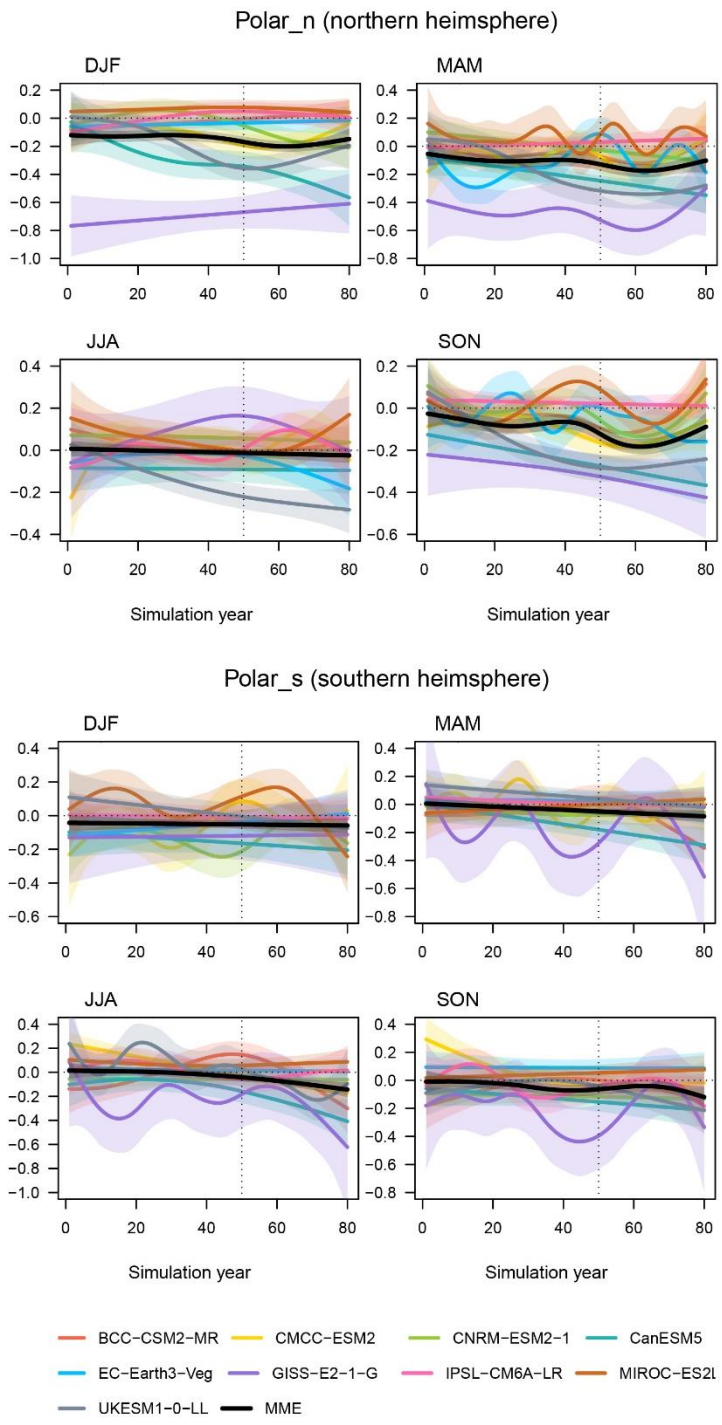

Figure S18. Seasonal changes in SPEI03 induced by deforestation averaged in the polar regions of the northern hemisphere (upper pane) and southern hemisphere (lower pane). The solid lines denote cubic spline regression, with significance indicated by colored areas at a level of 0.05.

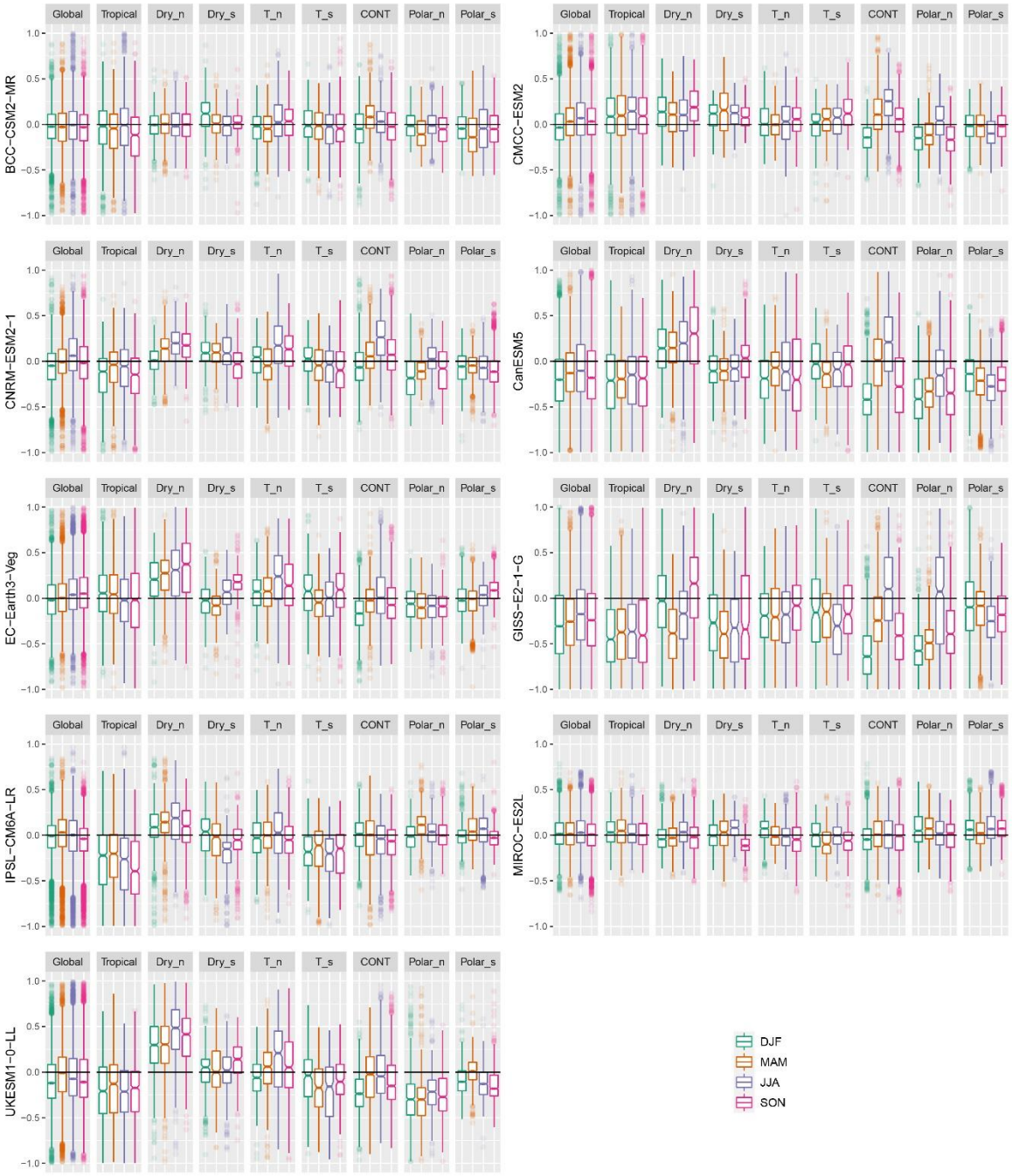

Figure S19. Box plots represent the seasonal (DJF, MAM, JJA, SON) changes in SPEI03 across different areas (global and eight regions) for individual model. Each box shows the interquartile range (IQR) of the SPEI03 changes within a specific region, with the lower and upper edges corresponding to the 25th (Q1) and 75th (Q3) percentiles, respectively. Outliers are also displayed and defined as values less than Q1-1.5x(IQR) or greater than Q3+1.5x(IQR). Different colors are used to represent different seasons.

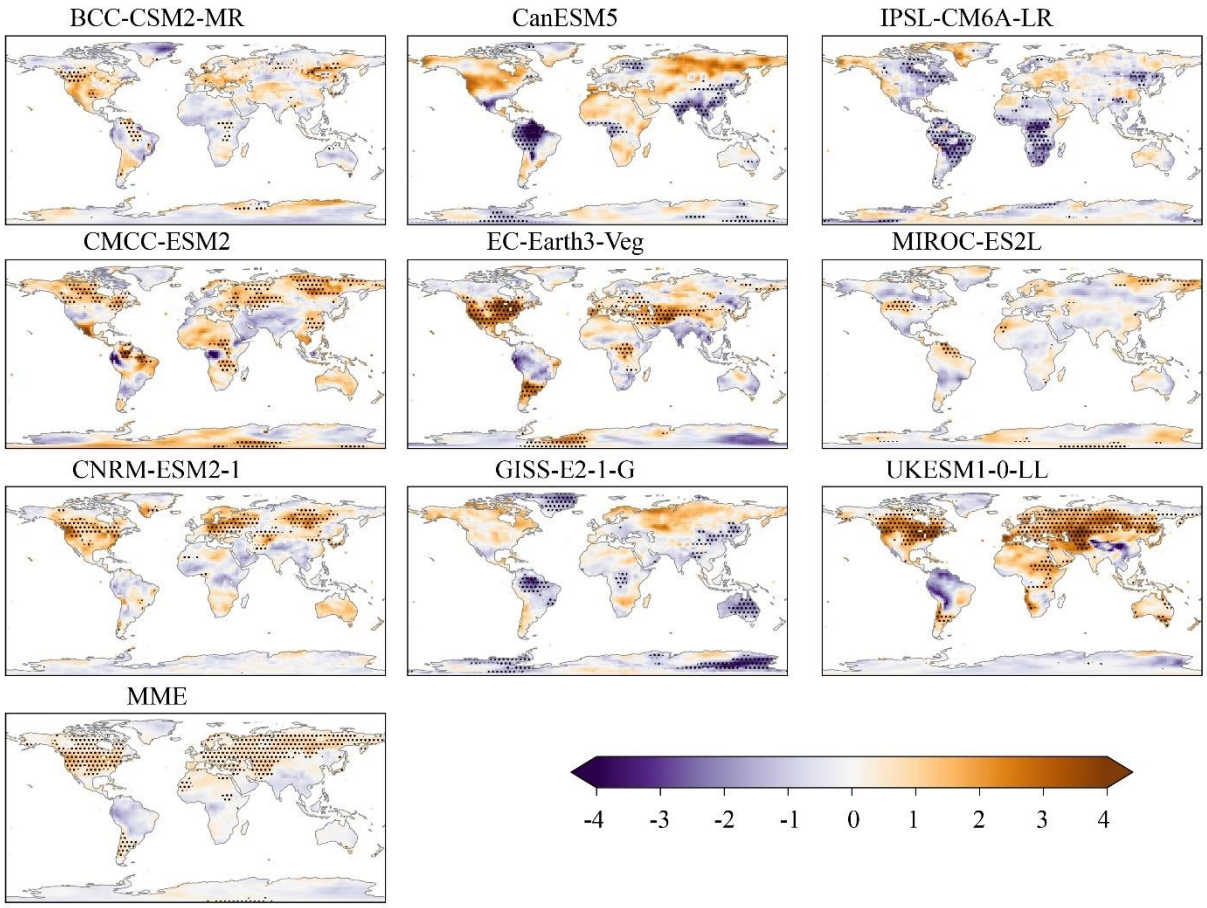

Figure S20. Global land-based cloud cover change (%) resulting from an idealized deforestation scenario (*deforest-global* minus *piControl*) for nine climate models (BCC-CSM2-MR, CMCC-ESM2, CNRM-ESM2-1, CanESM5, EC-Earth3-Veg, GISS-E2-1-G, IPSL-CM6A-LR, MIROC-ES2L, and UKESM1-0-LL), and their multi-model ensemble mean (MME) averaged for the last 30 years. The map shows the changes in the multi-year average of annual total precipitation, compared to *piControl* experiment. The black dots indicate the changes in precipitation, with significance tested using a two-tailed t-test at a p-value of 0.05.

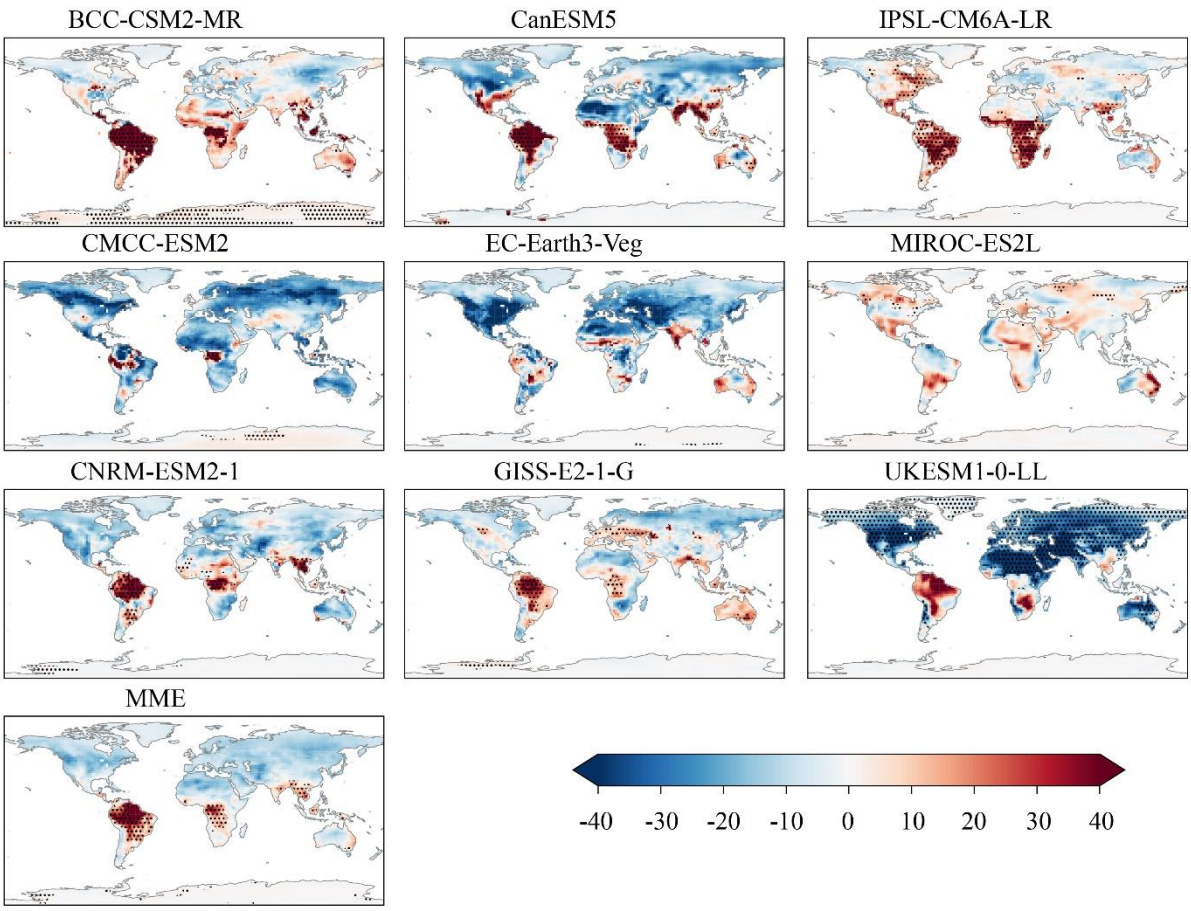

Figure S21. Global land-based potential evapotranspiration changes (mm yr^{-1}) resulting from an idealized deforestation scenario (*deforest-global* minus *piControl*) for nine climate models (BCC-CSM2-MR, CMCC-ESM2, CNRM-ESM2-1, CanESM5, EC-Earth3-Veg, GISS-E2-1-G, IPSL-CM6A-LR, MIROC-ES2L, and UKESM1-0-LL), and their multi-model ensemble mean (MME) averaged for the last 30 years. The map shows the changes in the multi-year average of annual potential evapotranspiration, compared to *piControl* experiment. The black dots indicate the changes in potential evapotranspiration, with significance tested using a two-tailed t-test at a p-value of 0.05.

Reference

Arora, V. K., and Coauthors, 2020: Carbon-concentration and carbon-climate feedbacks in CMIP6 models and their comparison to CMIP5 models. *Biogeosciences*, **17,** 4173-4222.

Berthet, S., R. Séférian, C. Bricaud, M. Chevallier, A. Voldoire, and C. Ethé, 2019: Evaluation of an Online Grid-Coarsening Algorithm in a Global Eddy-Admitting Ocean Biogeochemical Model. *J Adv Model Earth Sy*, **11,** 1759-1783.

Boucher, O., and Coauthors, 2020: Presentation and Evaluation of the IPSL-CM6A-LR Climate Model. *J Adv Model Earth Sy*, **12**.

Boussetta, S., G. Balsamo, A. Beljaars, T. Kral, and L. Jarlan, 2013: Impact of a satellite-derived leaf area index monthly climatology in a global numerical weather prediction model. *Int J Remote Sens*, **34,** 3520-3542.

Burton, C., and Coauthors, 2019: Representation of fire, land-use change and vegetation dynamics in the Joint UK Land Environment Simulator vn4.9 (JULES). *Geosci Model Dev*, **12,** 179-193.

Clark, D. B., and Coauthors, 2011: The Joint UK Land Environment Simulator (JULES), model description - Part 2: Carbon fluxes and vegetation dynamics. *Geosci Model Dev*, **4,** 701-722.

Coleman, K., and Coauthors, 1997: Simulating trends in soil organic carbon in long-term experiments using RothC-26.3. *Geoderma*, **81,** 29-44.

Collatz, G. J., M. Ribas-Carbo, and J. A. Berry, 1992: Coupled Photosynthesis-Stomatal Conductance Model for Leaves of C4 Plants. *Aust J Plant Physiol*, **19,** 519-538.

Craig, A., S. Valcke, and L. Coquart, 2017: Development and performance of a new version of the OASIS coupler, OASIS3-MCT_3.0. *Geosci Model Dev*, **10,** 3297-3308.

de Rosnay, P., J. Polcher, M. Bruen, and K. Laval, 2002: Impact of a physically based soil water flow and soil-plant interaction representation for modeling large-scale land surface processes. *Journal of Geophysical Research: Atmospheres*, **107,** ACL 3-1-ACL 3-19.

Decharme, B., and Coauthors, 2019: Recent Changes in the ISBA-CTRIP Land Surface System for Use in the CNRM-CM6 Climate Model and in Global Off-Line Hydrological Applications. *J Adv Model Earth Sy*, **11,** 1207-1252.

Delire, C., and Coauthors, 2020: The Global Land Carbon Cycle Simulated With ISBA-CTRIP: Improvements Over the Last Decade. *J Adv Model Earth Sy*, **12**.

Döscher, R., and Coauthors, 2022: The EC-Earth3 Earth system model for the Coupled Model Intercomparison Project 6. *Geosci. Model Dev.*, **15,** 2973-3020.

Farquhar, G. D., S. V. Caemmerer, and J. A. Berry, 1980: A Biochemical-Model of Photosynthetic Co2 Assimilation in Leaves of C-3 Species. *Planta*, **149,** 78-90.

Friend, A. D., and N. Y. Kiang, 2005: Land surface model development for the GISS GCM: Effects of improved canopy physiology on simulated climate. *J Climate*, **18,** 2883-2902.

Goudriaan, J., H. H. van Laar, H. van Keulen, and W. Louwerse, 1985: Photosynthesis, CO2 and Plant Production. *Wheat Growth and Modelling*, W. Day, and R. K. Atkin, Eds., Springer US.

Hajima, T., and Coauthors, 2020: Development of the MIROC-ES2L Earth system model and the evaluation of biogeochemical processes and feedbacks. *Geosci Model Dev*, **13,** 2197-2244.

Harper, A. B., and Coauthors, 2016: Improved representation of plant functional types and physiology in the Joint UK Land Environment Simulator (JULES v4.2) using plant trait information. *Geosci Model Dev*, **9,** 2415-2440.

Hasumi, H., 2006: CCSR Ocean Component Model (COCO) Version 4.0.

Hazeleger, W., and Coauthors, 2012: EC-Earth V2.2: description and validation of a new seamless earth system prediction model. *Climate Dynamics*, **39,** 2611-2629.

Ito, A., and T. Oikawa, 2002: A simulation model of the carbon cycle in land ecosystems (Sim-CYCLE): a description based on dry-matter production theory and plot-scale validation. *Ecol Model*, **151,** 143-176.

Ito, A., and M. Inatomi, 2012: Water-Use Efficiency of the Terrestrial Biosphere: A Model Analysis Focusing on Interactions between the Global Carbon and Water Cycles. *J Hydrometeorol*, **13,** 681-694.

Kelley, M., and Coauthors, 2020: GISS-E2.1: Configurations and Climatology. *J Adv Model Earth Sy*, **12**.

Koven, C. D., and Coauthors, 2013: The effect of vertically resolved soil biogeochemistry and alternate soil C and N models on C dynamics of CLM4. *Biogeosciences*, **10,** 7109-7131.

Krinner, G., and Coauthors, 2005: A dynamic global vegetation model for studies of the coupled atmosphere-biosphere system -: art. no. GB1015. *Global Biogeochem Cy*, **19**.

Li, W. P., and Coauthors, 2019: Development of Land Surface Model BCC_AVIM2.0 and Its Preliminary Performance in LS3MIP/CMIP6. *J Meteorol Res-Prc*, **33,** 851-869.

Lindeskog, M., A. Arneth, A. Bondeau, K. Waha, J. Seaquist, S. Olin, and B. Smith, 2013: Implications of accounting for land use in simulations of ecosystem carbon cycling in Africa. *Earth Syst Dynam*, **4,** 385-407.

Lovato, T., and Coauthors, 2022: CMIP6 Simulations With the CMCC Earth System Model (CMCC-ESM2). *J Adv Model Earth Sy*, **14**.

Oleson, K., and Coauthors, 2013: Technical description of version 4.5 of the Community Land Model (CLM).

*NCAR Technical Note NCAR/TN-503+STR***,** 169.
Olin, S., and Coauthors, 2015: Modelling the response of yields and tissue C : N to changes in atmospheric CO and N management in the main wheat regions of western Europe. *Biogeosciences*, **12,** 2489-2515.
Parton, W. J., J. W. B. Stewart, and C. V. Cole, 1988: Dynamics of C, N, P and S in Grassland Soils - a Model. *Biogeochemistry*, **5,** 109-131.
Roehrig, R., and Coauthors, 2020: The CNRM Global Atmosphere Model ARPEGE-Climat 6.3: Description and Evaluation. *J Adv Model Earth Sy*, **12**.
Rosenzweig, C., and F. Abramopoulos, 1997: Land-surface model development for the GISS GCM. *J Climate*, **10,** 2040-2054.
Séférian, R., and Coauthors, 2019: Evaluation of CNRM Earth System Model, CNRM-ESM2-1: Role of Earth System Processes in Present-Day and Future Climate. *J Adv Model Earth Sy*, **11,** 4182-4227.
Sellar, A. A., and Coauthors, 2019: UKESM1: Description and Evaluation of the U.K. Earth System Model. *J Adv Model Earth Sy*, **11,** 4513-4558.
Smith, B., D. Wårlind, A. Arneth, T. Hickler, P. Leadley, J. Siltberg, and S. Zaehle, 2014: Implications of incorporating N cycling and N limitations on primary production in an individual-based dynamic vegetation model. *Biogeosciences*, **11,** 2027-2054.
Swart, N. C., and Coauthors, 2019: The Canadian Earth System Model version 5 (CanESM5.0.3). *Geosci Model Dev*, **12,** 4823-4873.
Takata, K., S. Emori, and T. Watanabe, 2003: Development of the minimal advanced treatments of surface interaction and runoff. *Global Planet Change*, **38,** 209-222.
Takemura, T., H. Okamoto, Y. Maruyama, A. Numaguti, A. Higurashi, and T. Nakajima, 2000: Global three-dimensional simulation of aerosol optical thickness distribution of various origins. *Journal of Geophysical Research: Atmospheres*, **105,** 17853-17873.
Tatebe, H., Y. Tanaka, Y. Komuro, and H. Hasumi, 2018: Impact of deep ocean mixing on the climatic mean state in the Southern Ocean. *Sci Rep-Uk*, **8**.
Tatebe, H., and Coauthors, 2019: Description and basic evaluation of simulated mean state, internal variability, and climate sensitivity in MIROC6. *Geosci. Model Dev.*, **12,** 2727-2765.
Vancoppenolle, M., T. Fichefet, H. Goosse, S. Bouillon, G. Madec, and M. A. M. Maqueda, 2009: Simulating the mass balance and salinity of Arctic and Antarctic sea ice. 1. Model description and validation. *Ocean Model*, **27,** 33-53.
Wu, T. W., and Coauthors, 2019: The Beijing Climate Center Climate System Model (BCC-CSM): the main progress from CMIP5 to CMIP6. *Geosci Model Dev*, **12,** 1573-1600.
Wu, T. W., and Coauthors, 2013: Global carbon budgets simulated by the Beijing Climate Center Climate System Model for the last century. *J Geophys Res-Atmos*, **118,** 4326-4347.
Wyser, K., E. Kjellström, T. Koenigk, H. Martins, and R. Döscher, 2020a: Warmer climate projections in EC-Earth3-Veg: the role of changes in the greenhouse gas concentrations from CMIP5 to CMIP6. *Environ Res Lett*, **15**.
Wyser, K., T. van Noije, S. T. Yang, J. von Hardenberg, D. O'Donnell, and R. Döscher, 2020b: On the increased climate sensitivity in the EC-Earth model from CMIP5 to CMIP6. *Geosci Model Dev*, **13,** 3465-3474.
Yin, X. W., 2002: Responses of leaf nitrogen concentration and specific leaf area to atmospheric CO enrichment:: a retrospective synthesis across 62 species. *Global Change Biology*, **8,** 631-642.
Yool, A., E. E. Popova, and T. R. Anderson, 2013: MEDUSA-2.0: an intermediate complexity biogeochemical model of the marine carbon cycle for climate change and ocean acidification studies. *Geosci Model Dev*, **6,** 1767-1811.